Final Report

for

October 1989 - December 1993

Submitted to:

Defense Advanced Research Projects Agency

Grant # N00014-89-J-3122

Title: "Diagnostics and Modeling of Laser-Assisted MOCVD Growth of Thin Films"

Principal Investigator: W.L. Wilson, Jr.

Co-Principal Investigators: F.K. Tittel, N.J. Halas

Adjunct Associate: P. J. Wisoff

Address: Department of Electrical and Computer Engineering
Rice University
P.O. Box 1892
Houston, Tx, 77251
713-527-4804

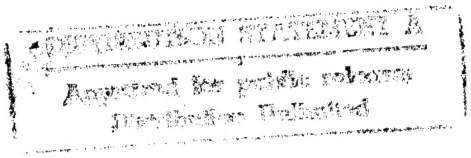

May, 1994

Objective

The objective of this work has been to develop new optical techniques that can be used to study the laser-assisted MOCVD growth of ZnSe thin films, and to characterize the high speed electronic properties of the epitaxial ZnSe material itself. Through the use of an ArF excimer laser at 193 nm, it is possible to photodissociate both precursors used for MOCVD growth of ZnSe, dimethylzinc (DMZ) and diethylselenium (DES). This technique permits epitaxial growth at reduced substrate temperatures and with much better control. This in turn leads to significantly improved film quality. Through a better understanding of the growth process, as well as a more detailed knowledge of the electronic characteristics of the material which is produced, it will be possible to better optimize and control the fabrication of high-quality ZnSe though laser-assisted MOCVD techniques.

Approach

The primary method used for investigating the dynamics of the laser-assisted growth technique has been vacuum ultraviolet (VUV) absorption spectroscopy. A tightly focused Nd-YAG laser is used to create an intense plasma in an Ar atmosphere. This plasma acts as a broad-band pulsed source of VUV radiation. By studying the absorption features in this broad-band spectrum as a function of time, it has been possible to determine the details of the photodisociation process of DMZ, and to measure the kinetics of the resulting photoproducts.

Results:

A modified reactor design has been completed and characterized. Using an inverted substrate growth configuration and the laser-assisted technique, ZnSe films with excellent optical properties have been grown. Using NH_3 as a dopant source and a post-growth anneal at about 700° C, p-type layers with active acceptor concentrations in the low 10^{18}

cm^{-3} range (as determined by C-V measurements) were obtained. The use of laser-assisted growth greatly enhances the properties of the material. A very simple and convenient UV-VUV source has been developed for making temporally and spatially resolved gas-kinetic measurements of the laser-assisted MOCVD process Using the focused pulse from a Q-switched Nd:YAG laser in an argon atmosphere we have developed a fast, broad-band light source which extends from the visible out 115 nm. Using this source, the photodissociation dynamics of dimethylzinc have been extensively studied. Briefly, upon irradiation with 193 nm photons from an ArF excimer laser, DMZ photo dissociates into a ground state zinc atom and two CH_3 radicals. The CH_3 radicals then undergo a two-body reaction to form C_2H_6 with a time constant of about 75 μsec under the experimental conditions similar to the growth conditions for making ZnSe films. The zinc atoms undergo no further kinetics, and diffuse to the growth surface. Since the methyl radicals combine with one another on such a short time constant little or no carbon-containing reactive species reach the growth surface. This implies that ZnSe films grown using the laser-assisted technique should be essentially carbon-free.

Other Accomplishment and Awards

P.J. Wisoff was given an Award of Excellence by the NCR Corporation. Furthermore, the one of the graduate students associated with this work, Mr. Joseph Elias was awarded the HARC Fellowship at Rice University for solid-state research. A second graduate student, Tracy Sharp has been named a Welch Fellow for this academic year.

Papers in refereed journals:

"A Tunable High Power Sub-Picosecond Blue-Green Dye Laser System with a Two-Stage Amplifier Design" by T.E. Sharp, C.B. Dane, F.K. Tittel, P.J. Wisoff, and G. Szabo *IEEE. J. Quantum Electron,* May 91 1221-1227.

"Dispersion Measurements of Single-Mode Fibers in the Blue Green Spectral Regions by an Interferrometric Method" by G. Szabo T.E. Sharp, F.K. Tittel and P.J. Wisoff. *IEEE J. Quantum Electron.* 1992.

"Ultrashort Laser Pulse Amplification in a XeF(C-A) Excimer Amplifier:" by T.E. Sharp, Th. Hofmann, C.B. Dane, W.L. Wilson, F.K. Tittel, P.J. Wisoff and G. Szabo.,*Optics Letters* (Dec 1990)

"Blue-Green Dye Laser Seeded Operation of a Terawatt Excimer Amplifier", by F.K. Tittel, Th. Hofmann, W.L. Wilson, T. Sharp P.J. Wisoff and G. Sazbo. *Topics in Physics,*_70, 441-451 (1972)

"Characteristics of an Ultrahigh Peak Power XeF(C→A) Excimer Laser System", by Th. Hofmann, T. Sharp, C. B. Dane, W.L. Wilson P. J. Wisoff, F.K. Tittel and G. Szabo, *IEEE J. Quantum Electronics,*_ JQE-28, 1336-1375 (1992).

"Quantitative Time-Resolved Observations of Ground-state Zinc Atoms, Methyl Radicals and Excited CH Radicals Resulting from the 193 nm Photodissociation of Dimethylzinc", Joseph Elias W.L. Wilson and P. Jeffrey Wisoff. *J. Appl. Phys.,* 74(11), 6962-6971 (1993)

"Photodissociation Dynamics of DMZn at 193 nm: Implications for the Growth of ZnSe Films by Laser-Assisted Metalorganic Chemical Vapor Deposition", by Joseph Elias W.L. Wilson and P. Jeffrey Wisoff. *J. Electronic Materials,* 23, 105-113 (1994)

Presentations

"Advanced Concepts of Lasers" F.K. Tittel, P. Canarelli, C.B. Dane, Th. Hofmann, G. Szabo, R. Sauerbrey, T. Sharp, W.L. Wilson, P.J. Wisoff and S. Yamaguchi, GCL8 in Madrid Spain, September 1990.

"Advanced Concepts for Blue-Green Lasers" F.K. Tittel, W.L. Wilson, and P.J. Wisoff Winter Quantum Electronic Meeting, Snowbird Utah, January 1990

"Amplification of High Intensity Ultrashort Blue-Green Laser Pulses using an XeF (C-A) Excimer Amplifier" C.B. Dane, T.E. Sharp, Th. Hofmann, W.L. Wilson, F.K. Tittel, P.J. Wisoff and G.Szabo, LEOS Annual Meeting, Boston, MA October 1990

"Optical Studies of the Photo-Dissociation of DMZn" , 6th Biennial Workshop of Organometalic Vapor Phase Epitaxy, Palm Springs, Ca, March (1993) W.L. Wilson, Joseph Elias and P.J. Wisoff.

"Optical VUV Studies of the Photo-Dissociation of Dimethyl Zinc for Laser Assisted MOCVD of ZnSe", Conference on Lasers and Electro-Optics, Baltimore Md., May (1993) by W.L. Wilson Joseph Elias and P.J. Wisoff

Honors

Joseph Elias - HARC Fellowship in Solid State Research
Tracy Sharp - Welch Fellowship for Graduate Study

Thesis Published:

Gregory B. Shinn Ph.D. "Laser-Assisted Metalorganic Chemical Vapor Deposition of Zinc Selenide"

Paul Mathew Gillespie. Ph.D. "Photoluminescence of Nitrogen-Doped Zinc Selenide by Photo-Assisted MOCVD."

Joseph A. Elias. M.S. "A Study of the Photodissociation Dynamics of Mimethylzinc and the Implications for the Growth of Zinc Selenide Films".

Apolak Borthakur M.S. "MOCVD Growth of p-Type ZnSe"

William Brian Haynes "Methods of Electrically Characterizaing ZnSe Epitaxial Layers on GaAs Substrates"

Graduate Students and Postdoctorals:

G. Szabo - Research Associate

Gregory Shinn - Graduate Student
Tracy Sharp - Graduate Student
Paul Gillespie - Graduate Student
Thomas Hofmann - Graduate Student
Joseph Elias - Graduate Student
Brian Hynes - Graduate Student
Apolak Borthakur - Graduate Student

Attachments:

Thesis Abstracts

Reprints of two most relevant papers

ABSTRACT

Laser-Assisted Metalorganic Chemical Vapor Deposition of Zinc Selenide

by

Gregory B. Shinn

Laser-assisted metalorganic chemical vapor deposition (LMOCVD) has been used to grow epitaxial zinc selenide at temperatures as low as 200 °C. The metalorganic sources, dimethylzinc (DMZ) and diethylselenide (DESe), were photodissociated with radiation from a 193 nm ArF excimer laser passing parallel to a (100) GaAs substrate. A two-stage purge scheme prevented deposition on the windows while minimizing disturbances to the gas flow in the growth region. The temperature dependence for both thermal and laser-assisted film growth was examined, keeping other reaction parameters fixed. The laser-assisted growth rate of ZnSe remained approximately constant at 1 μm/h over the temperature range 200-400 °C, temperatures at which no thermal growth occurs. At higher temperatures the thermally driven process was important and dominated the growth at temperatures above 500 °C. Photoluminescence analysis indicated that material grown at 400 °C by the laser-assisted process was of better quality than films grown by either method at other temperatures.

The effects of laser energy density and repetition rate on growth rate were examined. The growth rate at 20 Hz increased from 1.1 μm/h at 15 mJ per pulse laser energy to 2.5 μm/h with a 48 mJ pulse energy with all other reactor

conditions kept constant. Above a pulse energy of 40 mJ, the LMOCVD growth rates reached maximum values of about 2.7 μm/h and 4.6 μm/h for 20 Hz and 40 Hz operation, respectively. The rate was approximately doubled when the laser repetition rate was increased from 20 Hz to 40 Hz.

A two-level design of experiments matrix was done to examine the effect of six reactor parameters on film growth rate. Increases in substrate temperature, dimethylzinc partial pressure, diethylselenide to dimethylzinc source ratio and use of the laser all resulted in higher growth rate while increased reactor pressure was found to decrease the film growth rate.

A film grown with the laser radiation incident to the growth surface at a laser energy density of approximately 5 mJ/cm^2 exhibited the highest donor-bound exciton to self-activated center luminescence ratio of all films grown during this study.

Abstract

Photoluminescence of Nitrogen-Doped Zinc Selenide by Photo-Assisted MOCVD

by

Paul Matthew Gillespie

Zinc selenide is a wide band-gap (2.67 eV) II-VI compound semiconductor with potential use as a blue electro-optic device material. Problems with obtaining suitable p-type conductivity have limited device development. Zinc selenide epitaxial films, doped with nitrogen from NH_3, have been grown on gallium arsenide substrates by laser-assisted metal organic chemical vapor deposition (MOCVD). The effect of nitrogen doping was investigated with and without direct surface irradiation incident on the surface from a broad-band light source. Low temperature (8 K) photoluminescence spectroscopy has confirmed the incorporation of nitrogen as a shallow acceptor by the presence of acceptor-bound-excitons and associated donor-acceptor-pair recombination emissions. The MOCVD growth parameters have been optimized based on the presence of characteristic features in the photoluminescence spectra.

Growth rate mechanisms have been proposed for both laser-assisted MOCVD and direct-irradiation MOCVD. Simultaneous interaction of the two photo-assisted techniques show that direct irradiation of the surface does not enhance the growth rate under the laser-assisted condition. This confirms that direct surface irradiation

growth mechanisms involve the interaction of photo-generated carriers with alkyl groups from the precursors.

Abstract

Methods of Electrically Characterizing

ZnSe Epitaxial Layers on GaAs Substrates

by

William Brian Haynes

A number of different methods for electrically characterizing ZnSe thin films are presented. These include the Hall effect, current-voltage profiling, and capacitance-voltage profiling. The planar Schottky technique is used to analyze p-type ZnSe. The conductance method of Nicollian and Brews is applied for the first time to the ZnSe/GaAs MIS system to find the surface state density profile and the time constants associated with particular states. A novel photowash technique is used to make the GaAs surface gallium rich. Electron Paramagnetic Resonance is discussed in the context of probing thin film semiconductors. Room temperature mobilities for undoped, 1 μm, ZnSe films grown by Laser-assisted Metal Organic Chemical Vapor Deposition are as high as 309 $cm^2/V\text{-}s$. Mobilities at 77 K are limited by p-type GaAs conduction at the interface. Heterojunction barrier heights are found to be in the range of 0.6 - 0.9 eV and are probably due to interface traps. Schottky diode n-values are found to be high (>30) because of the heterojunction barrier. P-type conduction in the nitrogen-doped samples has not been found. Undoped ZnSe is n-type and is typically depleted of carriers. Surface state densities for both untreated and Ga-rich interfaces are found to be in the range of $10^{12}\ cm^{-2}\text{-}eV^{-1}$.

MOCVD Growth of p-type ZnSe

Apolak Borthakur

Abstract

Zinc Selenide (ZnSe) is a II-VI semiconductor with a wide (2.67 eV) bandgap that makes it a promising material for development of electro-optic devices in the blue-green region of the spectrum. The major research problem associated with ZnSe is the difficulty in doping it p-type. While there have been reports of good p-doped ZnSe grown by molecular beam epitaxy (MBE), there hasn't been any reliable reports of heavily doped p-ZnSe grown by metal organic chemical vapor deposition (MOCVD). MOCVD is a much cheaper process than MBE, has high throughput and can be used for mass production, and thus it is of great interest to investigate the development of ZnSe by MOCVD. We report here a technique for obtaining high quality p-doped ZnSe. Growth parameters have been optimized to yield p-doped ZnSe doped to as much as $7.9X10^{17}/cm^3$, which should be adequate for development of ZnSe blue-green LEDs.

ABSTRACT

A STUDY OF THE PHOTODISSOCIATION DYNAMICS OF DIMETHYLZINC AND THE IMPLICATIONS FOR THE GROWTH OF ZnSe FILMS

by

JOSEPH A. ELIAS

The dynamics of the ArF photodissociation of DMZn (dimethylzinc) have been studied. The implications of the results for the growth of ZnSe thin films are discussed. Time-resolved absorption profiles of ground state Zn and methyl radicals have been acquired using a plasma emission source. Time-resolved fluorescence from excited CH radicals has also been studied. The results indicate that the Zn concentration remains constant after the dissociating ArF pulse, indicating the system is a good source for free Zn atoms. The CH_3 radicals that are created recombine to form ethane, and simulations of the kinetics indicate that the concentration of methyl radicals reaching the substrate is insignificant. There was no indication of monomethylzinc formation. The CH radical is likely to combine with H_2 to form CH_3 within several microseconds. Thus the major sources for carbon contamination in the growth process (CH_3, MMZn, CH) are unlikely to reach the substrate.

Quantitative time-resolved observations of ground-state zinc atoms, methyl radicals, and excited CH radicals resulting from the 193 nm photodissociation of dimethylzinc

Joseph A. Elias, Peter J. Wisoff,[a] and William L. Wilson, Jr.
Department of Electrical and Computer Engineering, Rice Quantum Institute, Rice University, Houston, Texas 77005

(Received 11 February 1993; accepted for publication 18 August 1993)

The ArF laser photodissociation dynamics of dimethylzinc at 193 nm have been studied, and their implications for the growth of ZnSe thin films are discussed. A broadband, vacuum ultraviolet argon plasma emission has been used to acquire time-resolved absorption profiles from ground-state Zn atoms and methyl radicals. Time-resolved fluorescence from excited CH radicals has also been studied. The results indicate that the Zn concentration remains constant from 100 ns to 2 ms after the dissociating ArF pulse, indicating that this system is a good source for free Zn atoms. The CH_3 radicals are formed immediately after the dissociation pulse and recombine within several hundred microseconds to form ethane. There was no indication of monomethylzinc (MMZn) formation, and the detected CH radical is likely to combine with H_2 to form CH_3 within several microseconds. This implies that the major sources for carbon contamination in the growth process (CH_3, MMZn, CH) are unlikely to reach the growth surface.

I. INTRODUCTION

ZnSe is a direct, wide-band-gap, II-VI semiconductor with promising electro-optic applications, including blue lasers[1,2] and light-emitting diodes.[3,4] However, the quality of ZnSe films grown by metalorganic chemical-vapor deposition (MOCVD) is limited by defects introduced during the growth process.[5] It has been shown that lower growth temperatures reduce the number of defects.[6,7] Motivated by this, our group has grown ZnSe films at reduced substrate temperatures by using an ArF excimer laser to photodissociate the source gases.[8] More recently, this technique has been used to grow nitrogen-doped *p*-type ZnSe films by photodissociating NH_3.[9] While this laser-assisted MOCVD (LAMOCVD) method yields good quality ZnSe films, the fundamental chemistry of the dissociation process is not well understood. In the growth system, dimethylzinc (DMZn), diethylselenide (DESe), and ammonia (NH_3) are used as source gases for Zn, Se, and N atoms, respectively. Depending on the ultraviolet source, the dissociation of these precursors has been shown by other groups to break into intermediate compounds such as monomethylzinc (MMZn) (Ref. 10) and NH_2,[11] but the role of these intermediates in the growth process has not been studied. As a first step to addressing this question, this article concentrates on the 193 nm photodissociation dynamics of DMZn in a hydrogen atmosphere, and its implications for the growth of ZnSe films.

Since the growth of ZnSe by MOCVD involves several molecules, there are many possibilities for the intermediate chemistry. Depending on the energy supplied to the system, DMZn [$Zn(CH_3)_2$] may dissociate to either ($Zn+2CH_3$) or ($ZnCH_3+CH_3$), while the methyl radical itself, CH_3, can further dissociate to ($C+3H$), ($C+H+H_2$), ($CH+H_2$), (CH_2+H), etc. The intermediate radicals and/or atoms may also be found in excited states. For example, the Zn atom may appear in the ground state, initially occupy an excited state, or become ionized. Depending on the state of the atom, the Zn may react with other products in the reactor environment to form compounds such as ZnH, (Refs. 12 and 13) and be transported away from the growth region. Further complicating the picture is the possibility for recombination among the dissociation products to form compounds such as C_2H_6 or CH_4, as well as other reactions. If radicals such as CH_3 arrive at the growth surface and bond, the resultant carbon contamination could have serious consequences for the electrical properties of the semiconductor.[14,15] The role these intermediates play in the growth process needs to be explored in order to improve the overall control and quality of LAMOCVD ZnSe films.

Previously, mass spectrometry has been used to determine the photofragments of the dissociation process.[16] Quantitative results from this technique are dependent on knowing the ionization quantum efficiencies of the molecules and atoms that are observed. Qualitatively, the products detected in mass spectrometry studies have to be distinguished between neutral photoproducts that are ionized in the ion chamber and ions formed in the dissociation process. Mass spectrometry studies are limited in temporal resolution, in that most experiments detect only byproducts of a photodissociation processes, after photoproduced radicals have recombined or reacted with other species. Laser-induced-fluorescence (LIF) studies have also been used to qualitatively identify photoproducts;[17] however, this technique is generally limited to probing reactants that have transitions in the visible, due to the availability of suitable laser sources. The photodissociation of the source gases of interest here yields atoms and/or radicals which

[a]Present address: NASA, JSC, Houston, TX 77058.

 0021-8979/93/74(11)/6962/10/$6.00

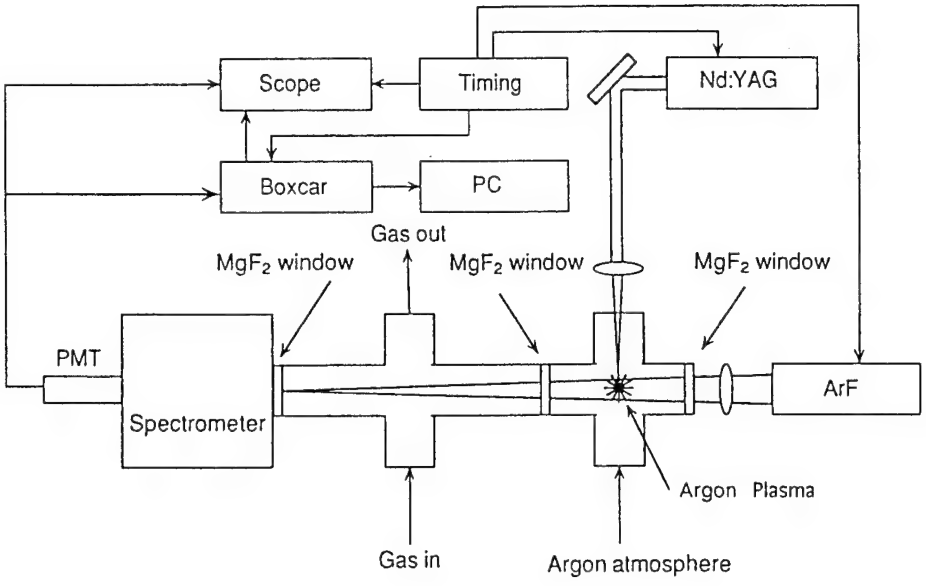

FIG. 1. Top view of the experimental layout. The experiment consists of a photodissociation laser (ArF), a laser (Nd:YAG) to create the plasma probe source, a 0.25 m spectrometer, a solar-blind PMT, a gated boxcar integrator, a timing control generator, an oscilloscope, and a microcomputer.

have electronic transitions in the VUV-VIS wavelength range. In this study, a pulsed broadband VUV light source has been used to apply noninvasive photoabsorption techniques to analyze the photodissociation products of the $DMZn+H_2$ system. Quantitative, time-resolved studies are presented.

II. DESCRIPTION OF THE DISSOCIATION-PROBE SYSTEM

In order to study the growth process of ZnSe on GaAs substrates, a special reaction cell was constructed. As shown in Fig. 1, an ArF laser (Questek, Model 2220, operating at 5 Hz, 100 mJ/pulse) is focused into a stainless-steel absorption cell, which contains DMZn in a hydrogen ambient atmosphere. This is similar to the geometry which is used in the actual LAMOCVD growth cell, where the ArF beam profile is focused approximately 0.5 cm above the surface of the GaAs substrate. The DMZn (Texas Alkyls, 99.9995%) is obtained from a bubbler immersed in a constant temperature bath. Extra dry hydrogen is passed through a palladium diffuser and is used as the carrier gas. A control system interacting with mass flow controllers and pressure controllers allows for separate adjustment of the flow rate, metal-organic partial pressures, and the total system pressure. Hydrogen is passed over the windows of the absorption cell to prevent unwanted metal deposition. The purge flow rate is maintained around 50 times the metal-organic flow rate.

In order to determine the species created in the ArF dissociation of DMZn, an absorption-probe experiment was designed using a novel plasma light source.[18] The plasma is created by focusing a Nd:YAG laser (Spectra Physics, Quanta Ray Model DCR-3, operating at 5 Hz, 0.8 J/pulse) into a stainless-steel plasma cell containing an argon atmosphere at several hundred Torr of pressure. This plasma emits a temporally short broadband continuum of radiation due mainly to free-free transitions (bremsstrahlung) in the Ar. The plasma emission is used to back light the absorption cell, allowing absorption studies of the products that are formed due to the photoabsorption of the ArF laser photons. By varying the timing between the ArF laser pulse and the Nd:YAG laser pulse (and thus the plasma emission), the temporal dependence of the absorption profile is acquired. The plasma emission is also detected from a side window at the plasma cell by an UV-VIS photodiode (Hamamatsu R1193U-02). This is used to normalize the signal detected at the spectrometer in order to account for shot-to-shot variation in the plasma intensity.

The plasma cell is separated from the absorption cell by a MgF_2 window which transmits wavelengths longer than $\lambda \sim 1150$ Å. Typical spectral features of the plasma emission from 1000 to 2500 Å are shown in Fig. 2. The spectrum is a mixture of continuum and line emission, mostly from Ar II and Ar III. The temporally short (~ 200 ns) plasma emission allows for good time resolution of the absorption profiles. The intensity of the emission is low, thus the plasma does not induce further photodissociation processes. Similar plasma sources have been used to perform spectroscopy and excitation of alkali halide and rare-gas alkali molecules.[19,20]

The ArF dissociating beam and the plasma are centered on the optical axis of the spectrometer, as shown in Fig. 3. The ArF laser beam is focused with a 1 m focal length CaF_2 lens and is directed slightly off axis onto a beam block to prevent most of the 193 nm radiation from entering the spectrometer. This alignment allows for maximum spatial overlap of the dissociating beam and the plasma. The DMZn molecule has a large cross section for absorption around 193 nm,[21] and is readily dissociated by

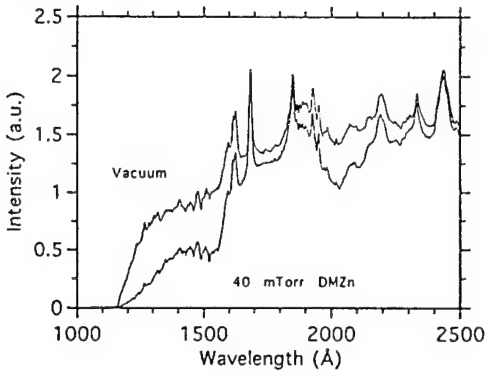

FIG. 2. Typical spectral output of the plasma emission from 1000 to 2500 Å. The upper trace is the detected plasma spectrum with vacuum in the absorption cell, and the lower trace is the detected plasma spectrum with 40 mTorr of DMZn in the absorption cell. Two broadband absorptions can be seen, one around 2000 Å (near the wavelength of the ArF laser), and another in the deep VUV from 1200 to 1600 Å. The peaks in both spectra are line emission from ionized argon, mainly Ar II and Ar III, while the broad continuum is due mainly to free-free transitions, or bremsstrahlung.

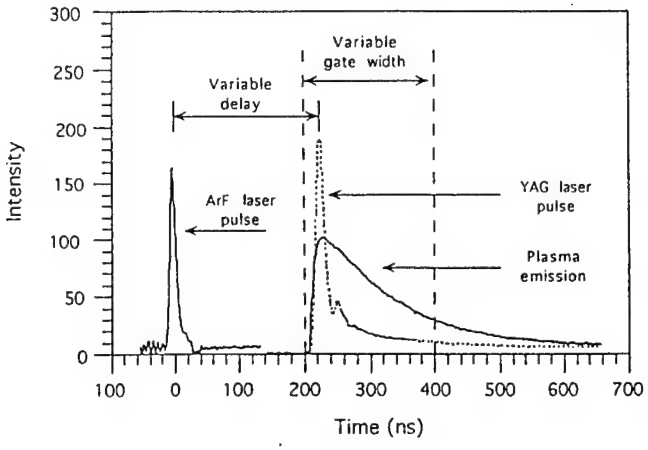

FIG. 4. Timing diagram showing relationship between the ArF laser pulse, the Nd:YAG laser pulse, the plasma emission, and the boxcar gate. The timing between the ArF laser pulse and the plasma emission can be varied from zero delay to several seconds delay, if necessary. Due to flow of undissociated DMZn into the optical column, the upper limit on the time resolution is ~2 ms. The lower resolution of the timing is limited by the inherent jitter of the ArF laser (±25 ns). The boxcar gate width can be varied down to 5 ns. It is found that the best repeatability of the data is obtained with 200 ns gate widths. It should be noted that, in the figure, the relative intensities of the ArF laser pulse, the YAG laser pulse, and the plasma emission are not to scale.

the ArF laser photons. The laser-beam profile has a rectangular cross section and the area measures 0.285 cm^2 (3×9.5 mm^2) at the center of the dissociation region in the absorption cell. The energy density of the beam can be varied from ~250 mJ/cm^2 (12 MW/cm^2) down to ~20 mJ/cm^2 (1 MW/cm^2).

The timing between the dissociating beam and the plasma probe is controlled by a digital pulse generator (Stanford Research Systems Model DG-535). The detection system consists of a 0.25 m vacuum spectrometer (Acton Research Model VM502), to which a solar blind photomultiplier tube (PMT) (Hamamatsu R1080) is attached. A typical slit width is 100 μm, yielding a wavelength resolution of ~4 Å. The signal from the PMT is processed by a boxcar integrator (SRS 245, 250) and the data are recorded with a microcomputer. The temporal relation of the plasma emission, the ArF pulse, and the boxcar gate is shown in Fig. 4. The timing resolution of the system is limited by the jitter of the ArF laser discharge, which for our laser is ±25 ns. Due to the flow of undissociated DMZn back into the optical column, the maximum delay time from the dissociating laser for probing photoproducts is ~2 ms.

III. ABSORPTION EXPERIMENTS

Two photoproducts were detected as a result of the photodissociation of DMZn by a focused ArF laser beam.

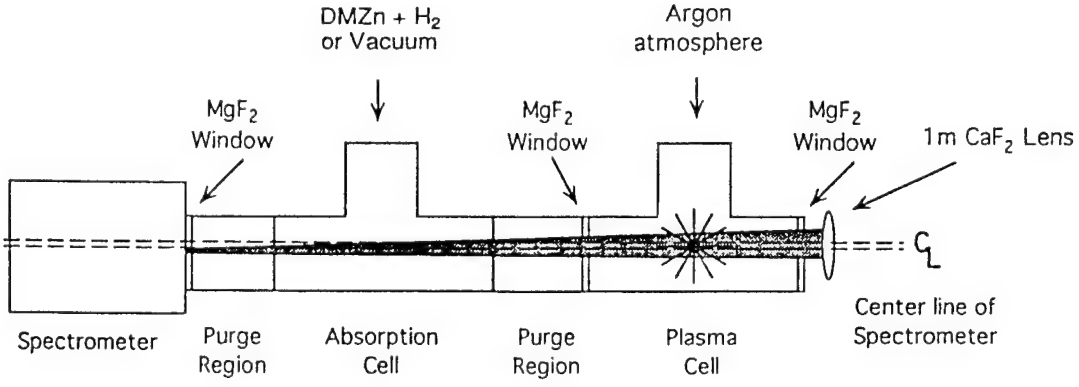

FIG. 3. Side view of the experiment. The ArF laser beam enters from the right-hand side and is focused slightly off axis by a 1 m CaF_2 lens into a beam block, which prevents most of the 193 nm radiation from entering the spectrometer. The Nd:YAG laser enters the plasma cell orthogonal to the ArF laser beam and creates the Ar plasma, which is used to back light the absorption cell to obtain time-resolved absorption profiles of the fragments made in the photodissociation process. The absorption cell and plasma cell are separated by a MgF_2 window which allows wavelengths longer than $\lambda\sim1150$ Å to be transmitted. The absorption cell is operated at a typical pressure of 25 Torr of $DMZn+H_2$; the plasma cell operates at several hundred Torr of argon, and the spectrometer is kept at vacuum.

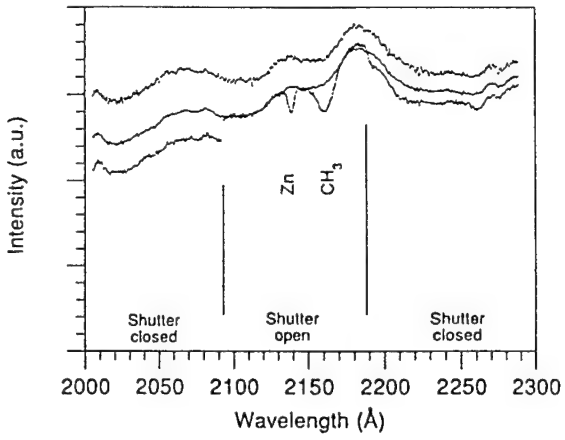

FIG. 5. Absorption profiles of Zn and CH_3. Curve A is the detected plasma spectrum with vacuum in the absorption cell, curve B is an empirical fit to the base line of the absorption curve, and curve C is the detected plasma spectrum with DMZn in the absorption cell. Curve C is separated into three regions: (1) the ArF laser on, but with the output baffle shut; (2) the ArF laser on, with the output baffle open; and (3) the ArF laser on, and the output baffle shut. This was done so as to eliminate the effect of any noise in the data due to the firing of the ArF thyratron, and to observe the variation in the spectra due to the broadband DMZn absorption.

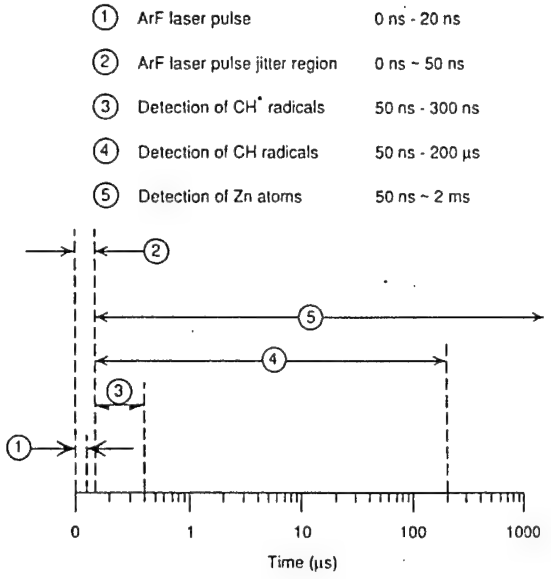

FIG. 6. Summary of the photospecies and the time scales involved. Zinc atoms and methyl radicals are detected in absorption, along with CH* radicals detected in emission. The region from 0 to 50 ns is noisy due to stray 193 nm light entering the spectrometer.

These are ground-state Zn and ground-state methyl radicals, as is seen in Fig. 5. The transitions shown are the $(4\,^1P_1) \leftarrow (4\,^1S_0)$ transition at 2139 Å for Zn,[22] and the $B \leftarrow X$ transition at 2160 Å for CH_3.[23] Two other transitions of CH_3 were detected, the $C \leftarrow X$ transition of CH_3 at 1503 Å, as well as an absorption at 1385 Å, which may be due to the $\delta_2 \leftarrow X$ and $\gamma_2 \leftarrow X$ transitions of CH_3.[23] The CH_3 transition at 2160 Å was used to determine the methyl radical concentration. Excited CH radicals were also detected in emission at 4315 Å. A summary of the species detected and the relevant time scales is shown in Fig. 6, where the transitions detected are

$$\begin{aligned} &\text{Zn} \quad (4\,^1P_1) \leftarrow (4\,^1S_0), \quad \lambda = 2139 \text{ Å}, \\ &\text{CH}_3 \quad B \leftarrow X, \quad \lambda = 2160 \text{ Å}, \\ &\text{CH}^* \quad A \rightarrow X, \quad \lambda = 4315 \text{ Å}. \end{aligned} \tag{1}$$

The results from the absorption experiments are discussed below, and the results from the fluorescence experiments are discussed in Sec. IV.

Because of the hydrogen window purge, the effective length of the absorption region in the cell had to be determined. This was accomplished by measuring the broadband DMZn absorption with no purge gas flowing, and comparing it to the absorption measured with the purge gas flowing. By this method, it is found that the average absorption path length in the cell with the hydrogen purge flowing is $L = 7 \pm 1$ cm.

The cross section of absorption for DMZn has been reported by several groups.[21,24,25] As shown in Fig. 7, the cross section obtained in this work is in good agreement with the results of the other groups. The absorption feature centered around 2020 Å has a peak cross section of approximately 0.3 Å^2, close to the value obtained by Fujita and co-workers[24] and Ibuki and co-workers[25] whereas the maximum obtained by Chen and Osgood[21] at this wavelength is 0.4 Å^2. Comparing our results to those of Ibuki and co-workers, the deeper UV feature centered at ~1550 Å is in good agreement with a maximum of ~0.7 Å^2. However, the feature at ~1200 Å yields a maximum of ~1.6 Å^2, compared to a maximum of ~1.1 Å^2 for Ibuki and co-workers.

In order to calculate the concentrations of absorbers (either Zn or CH_3) from the absorption profiles, it is necessary to estimate the relative depth of the absorptions. An empirical estimate of the base line of the absorption curve is calculated to compensate for the broadband absorption due to the DMZn molecule. This is necessary because as the ArF dissociates the DMZn in its optical path, the broadband molecular absorption decreases, and thus the

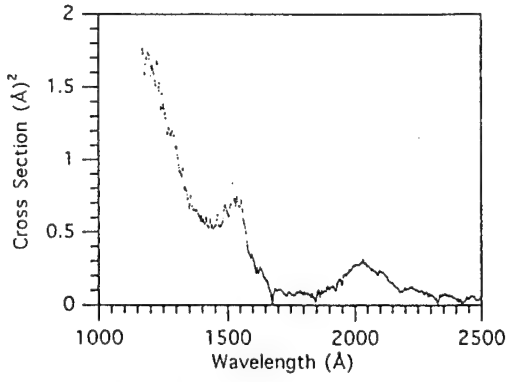

FIG. 7. Absorption cross section for DMZn from 1150 to 2500 Å. The peaks have been identified by Ibuki and co-workers (Ref. 25) as the Rydberg transitions $4p \leftarrow 2a_1''$ (~2020 Å), $4p \leftarrow 3a_1'$ (~1520 Å), and $3p \leftarrow 2e$ and/or $3p \leftarrow 2e''$ (~1180 Å).

TABLE I. List of rate constants from Ref. 30.

	Reaction	k (300 K) $(cm^3)/(molecule\ s)$	k (673 K) $(cm^3)/(molecule\ s)$
I	$CH_3+H_2 \rightarrow CH_4+H$	1.2×10^{-20}	4.7×10^{-16}
II	$CH_3+H \rightarrow CH_4$	2.0×10^{-10}	1.5×10^{-10}
III	$CH_3+CH_3 \rightarrow C_2H_6$	4.4×10^{-11}	2.6×10^{-11}
IV	$C_2H_6 \rightarrow CH_3+CH_3$	5.2×10^{-49} [a]	7.2×10^{-13} [a]

[a]Units for unimolecular reaction rate coefficient: $cm^6/(molecules^2\ s^2)$.

signal to the spectrometer increases. As more DMZn dissociates (by increasing the ArF energy), the detected spectrum more closely resembles the vacuum spectrum. From this fit, as shown in Fig. 5, the observed concentration of both Zn atoms and CH_3 radicals can be calculated.

To determine the density of CH_3 absorbers in the optical column, the time decay of the methyl radical absorption is recorded, and gas kinetics are used to determine the initial concentration of radicals present. Based on the rate constants listed in Table I, the dominant reaction for the removal of CH_3 is the recombination reaction: $CH_3+CH_3+M \rightarrow C_2H_6+M$. The reaction to form ethane is kinetically favorable over the formation of methane. It has also been shown[26,27] that ethane is the major product of the recombination of methyl radicals in the photolysis of DMCd.

The decay of the methyl radical absorbance signal at 2160 Å versus time is shown in Fig. 8. In order to determine the density of absorbing radicals N, the kinetic equations for a second-order reaction are used,[28]

$$\frac{dN}{dt}=-2kN^2. \tag{2}$$

Rearranging and integrating,

$$N=\frac{N_0}{2kN_0t+1}. \tag{3}$$

From Beer's law, the absorbance

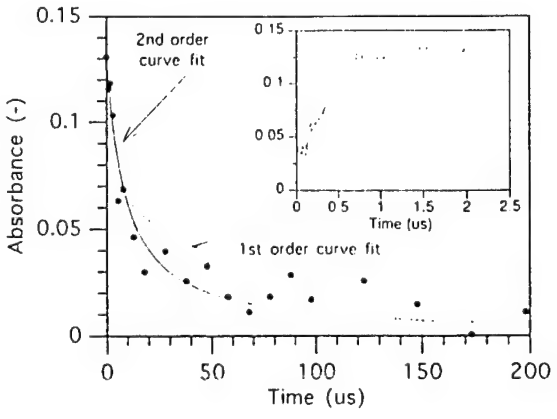

FIG. 8. Decay of the CH_3 absorbance ($B \leftarrow X$ transition at 2160 Å). The initial point was taken at the peak absorption, which corresponded to a time of $t=2$ μs. The inset shows the buildup of methyl radicals prior to $t=2$ μs.

$$A=\ln\frac{I_0}{I}=N\sigma L. \tag{4}$$

Combining Eqs. (3) and (4),

$$A=N\sigma L=\frac{A_0}{A_0Kt+1}, \tag{5}$$

where $K=2k/\sigma L$ and $A_0=N_0\sigma L$. Equation (5) is then used to fit the CH_3 absorbance signal decay. From the curve fit, the constant K is determined. To determine N_0, the term σL must be found from the relations in Eq. (5),

$$\sigma L=\frac{2k}{K} \quad \text{and} \quad N_0=\frac{A_0}{\sigma L},$$

where k is the known rate constant of the recombination rate for methyl radicals to form ethane, and A_0 is the initial absorbance. Similar to the results of Callear and van den Berg[29] the methyl radical absorption does not peak until several microseconds after the dissociation. This is attributed to methyl radicals initially appearing in an excited state, which are then collisionally relaxed to the ground state. For the present work, the methyl radical absorption peaks at $t=2$ μs relative to the ArF laser pulse.

Both the reaction kinetics and the change in the broadband DMZn absorption indicate that, at the energy densities in these experiments, approximately half of the DMZn is being dissociated. Referring to tabulated rates on the production of ethane from the recombination of methyl radicals,[30] $k=4.4\times10^{-11}$ molecules^{-1} cm^3 s^{-1} at room temperature. For the data shown in Fig. 8 and its curve fit, the constant K is found to be $K=0.856$ μs^{-1}. The rate constant k and curve fit constant K are then substituted back into Eq. (5). This gives $\sigma L \simeq 1.03\times10^{-16}$ cm^3, which yields $N_0=1.28\times10^{15}$ cm^{-3}. This compares with the known initial concentration of DMZn, $N_{DMZn}=1.30\times10^{15}$ cm^{-3}, calculated from flow rates and pressures of the gas delivery system and confirmed by the good agreement with other groups on the DMZn cross-section measurements. The calculated absorption density is consistent with the observed spectra, since a significant broadband attenuation of the DMZn molecule is still present as is seen in curves B and C of Fig. 5. Curve B shown in the figure represents the broadband attenuation due to ~60% of the DMZn remaining undissociated.

The effect of ArF energy fluence on the methyl absorption signal was also measured. The plot of CH_3 absorbance versus ArF energy is shown in Fig. 9. The absorbance follows a typical exponential saturation dependence described by

$$g(F)=K(1-e^{-\sigma F}), \tag{6}$$

where g is the absorbance, F is the energy fluence, σ is the absorption cross section (in cm^2/mJ), and K is a constant. The saturation point is defined as that fluence F_{sat} where σF equals unity. From the curve in Fig. 9, $F_{sat} \sim 75$ mJ/cm^2. This compares with a calculated value of

$$F_{sat}=\frac{h\nu}{\sigma}=68 \text{ mJ/cm}^2. \tag{7}$$

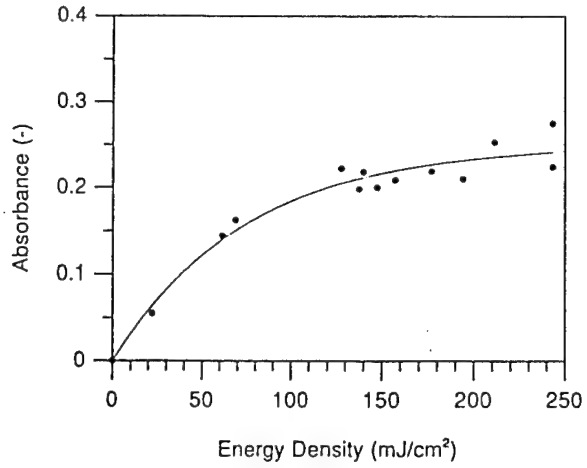

FIG. 9. Absorbance of CH_3 (at 2160 Å) vs ArF energy. The absorbance curve has a saturation point around 75 mJ/cm^2. The saturation energy density for DMZn irradiated by an ArF laser is calculated to be $E_{sat}=64$ mJ/cm^2.

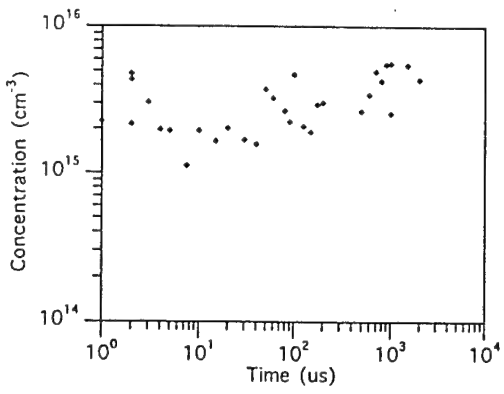

FIG. 10. Observed Zn concentration vs time. The concentration is calculated from the equivalent width of Zn, and a "curve of growth." Equivalent widths are obtained from the difference in the areas of curve B and curve C from 2134 to 2144 Å in Fig. 7.

To extract the density of absorbing Zn atoms in the optical column, the equivalent width of the Zn resonant absorption line is analyzed. Following Corney,[31] one can show for optically thick absorbing columns, the number of absorbing atoms N is given by

$$N=\frac{(W_\omega)^2\epsilon_0 mc}{\pi e^2 f_{ik} L\Gamma}, \tag{8}$$

where L is the absorption length (m), Γ the resonant linewidth (s^{-1}), f_{ik} the absorption oscillator strength, and W_ω the equivalent width (s^{-1}). However, when the gas is not in a high-pressure regime, the line shape is described by a combination of Gaussian (Doppler broadened) and Lorentzian (pressure broadened) linewidths. In this case, in order to determine the number of absorbers, a "curve of growth" is used.[31] Using the oscillator strength of the zinc absorption transition, $gf=1.3$,[32] the Doppler broadening has a value of $\Delta=2.15$ GHz. The pressure broadening comes from natural ($\Gamma_1=118$ MHz) and hydrogen-pressure broadening ($\Gamma_2=33$ MHz). Taking their ratio and applying it to the curve of growth gives a Zn concentration of a few 10^{15} cm^{-3}. Although there is some scatter to the data, the observed Zn concentration shows no trend either up or down over a time regime extending from 100 ns to 2 ms after the dissociation pulse as shown in Fig. 10. This indicates that the Zn atoms were not reacting with any other species to form intermediate compounds over this time period. Any intermediate compound that would consume Zn (such as ZnH) would have to be formed within the first 50 ns or have a lifetime longer than several milliseconds.

IV. FLUORESCENCE EXPERIMENTS

The photodissociation of DMZn by 193 nm radiation also produced a blue fluorescence centered around 4315 Å. In order to determine the source of this emission, a slightly different experimental arrangement was employed. The solar blind PMT was replaced by an UV-VIS detector (either Hamamatsu PMT 6199 or R943-02) that has a wide spectral response. In order to obtain good signal-to-noise ratios, the slits on the spectrometer were opened from 350 to 750 μm, depending on the concentration of DMZn and the type of PMT.

The blue emission, shown in Fig. 11, is due to the CH ($A\,^2\Delta \rightarrow X\,^2\Pi$) transition.[33] The resolution of the data in the figure is 6 Å and the some of the features of the P, Q, and R branches of the transition are evident. A plot of the decay of CH* versus time is shown in Fig. 12. Using an exponential curve fit, the upper state lifetime τ of the A state is estimated to be $\tau \sim 80$ ns. This compares with the published radiative lifetime of $\tau \sim 540$ ns,[34] as an average of several of the rotational bands of CH*. Thus the upper state decay of CH* in our system is mainly nonradiative collisional deexcitation.

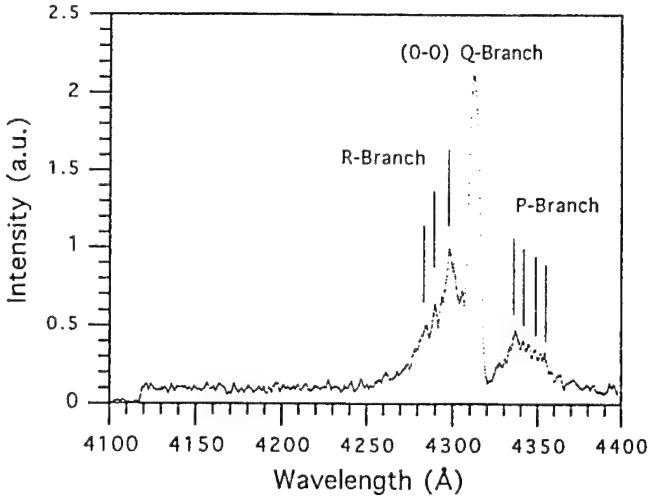

FIG. 11. Emission from the $A \rightarrow X$ transition of the CH radical. The peak at 4315 Å is due to the 0-0 Q-branch transition, and the P-branch and R-branch vibrational transitions are also evident. Also of note is the lack of emission at 4128 or 4176 Å which are identified with the $A \rightarrow X$ transitions of MMZn. The resolution of the spectrometer for these experiments was 10 Å.

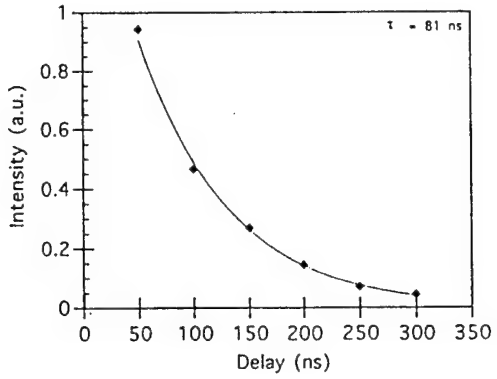

FIG. 12. Decay of the Q-branch emission from CH*. The decay curve fits an exponential decay which gives $\tau \sim 80$ ns.

V. DISCUSSION

A. Absorption and fluorescence results

The observed ground-state Zn concentration is approximately that which one would expect from the amount of DMZn which is photodissociated by the incident 193 nm laser pulse. No other transitions of Zn are detected, either from its ground state or its ionic state. There is a possibility that some Zn is being formed in the $4\,^3P_1$ metastable state, but the yield to that state has been shown to be small by Yu *et al.*[35] In the present work, there are no indications of the formation of intermediate compounds such as MMZn or ZnH. Others have explored the MMZn radical by absorption[36] and LIF.[37] For DMZn photodissociation, it has been established that the emission at $\lambda = 4128$ Å and $\lambda = 4176$ Å (noticeably absent in Fig. 11) is due to the $A \rightarrow X$ band of MMZn. There is no detected emission in the present experiments from these transitions or any of the other known transitions of MMZn,[36] $\lambda = 2671$ Å and $\lambda = 2739$ Å. A set of experiments was also carried out to look for the monomethyl fragment in absorption at these wavelengths and no signal was found. The photosensitized reaction to form ZnH [$Zn(4\,^3P_1) + H_2 \rightarrow ZnH$] has also been explored.[38,39] No signal was detected in this work in the regions identified for ZnH emission.[38,40] The lifetime of ZnH has been shown to be approximately 10 μs.[38] Any ZnH that is formed would decay to ground-state Zn and hydrogen, and a change in the Zn concentration would be observed on a 10 μs time scale. As discussed previously, no change in the Zn concentration was observed over several milliseconds, so it is unlikely that any photosensitized reaction to form ZnH consumes an appreciable number of Zn atoms. Therefore, it can be inferred that most of the Zn is being formed in a ground state, and that if there is the formation of another state of Zn, it does not have an appreciable effect on the growth process.

The absorption experiments also show the formation of ethane from the recombination of methyl radicals, which has important implications on the incorporation of carbon in the films. The methyl radicals recombine to form ethane on the order of a few hundred microseconds, indicating that the methyl radicals do not have time to reach the growth surface and bond. Ethane also does not absorb 193 nm radiation,[41] thus one would not expect the ethane that has been formed by the recombination of methyl radicals to be dissociated by the next ArF pulse. The formation of ethane from methyl radicals also has important consequences for ZnSe MOCVD growth. Fujita *et al.*[42,43] attributed higher photoassisted growth rates of ZnSe to the elimination of the alkyl groups from the precursor gases. The same group has also proposed that UV-induced oxidation-reduction mechanisms on the surface of the substrate leads to the elimination of alkyls from the substrate surface, thus lowering the carbon contamination in the films. This is in qualitative agreement with Giapis *et al.*,[44] who showed with secondary-ion-mass spectroscopy (SIMS) and photoluminescence (PL) data analysis that carbon incorporation in ZnSe films was lowered by changing the Se precursor from MASe to DESe. The PL spectra from the films grown by our LAMOCVD method show there is no I_c peak located at 2.7920 eV, which is one indication that C contamination is not present in significant concentrations in the films.

The results of the fluorescence experiments show that CH* is being produced, but its concentration has not been determined. The reactivity of CH is substantial due to the fact that it has two dangling bonds. Once the CH* decays to its ground state (within 300 ns), it would react very quickly. Braun, Bass, and Pilling[45] showed that CH radicals react very efficiently with H_2 in the reaction: $CH + H_2 \rightarrow CH_3$, which is first order in CH. For typical H_2 concentrations in our experiments ($\sim 8 \times 10^{17}$ cm^{-3}), the CH would essentially be consumed within several microseconds; therefore, it is unlikely that any unreacted CH radicals reach the growth surface. The formation of methyl radicals from CH is dependent on an excess of H_2. Growth systems that use inert gases (such as He) to transport the metalorganics would expect ethylene as a major byproduct of the reaction of CH + CH (see Braun and co-workers[45]).

The absorption experiments have identified the dissociation kinetics and concentrations of methyl radicals and Zn. The fluorescence of CH radicals is indicative of a high-energy density system, but it does not seem likely to be a channel for C incorporation in the films. The constant concentration of Zn atoms over time and the absence of MMZn and ZnH indicates that these two radicals are not a major concern for the growth system.

B. Energy dependence results

The energies required to dissociate DMZn and form various photoproducts are listed in Table II, and shown schematically in Fig. 13. An ArF photon contains 6.42 eV of energy, so a single photon is able to photodissociate a DMZn molecule to create one Zn atom and two CH_3 radicals. This leaves an excess of ~ 2.59 eV which would be distributed among the photoproducts. Since we observe the formation of ground-state Zn immediately (within 100 ns of the ArF pulse) and we do not detect MMZn, this implies that any intermediate radical (such as MMZn) is either short lived (within 50 ns of the ArF pulse) or very long lived (several milliseconds). The possibilities for the

TABLE II. Energies of reactions.

	Dissociation reaction	Energy (eV)	Reference
I	$Zn(CH_3)_2 \rightarrow Zn(CH_3)+CH_3$	2.76	54
II	$Zn(CH_3) \rightarrow Zn+CH_3$	1.06	54
III	$CH_3 \rightarrow H+CH_2$	4.9	23
IV	$CH_2 \rightarrow H+CH$	4.3	23
V	$CH(A\,^2\Delta) \rightarrow CH(X\,^2\Pi)$	2.87	35 and this work
	total required energy:	15.89	
	$h\nu$ (193 nm):	6.42	

excess energy from the first photon are: (i) creating excited-state Zn, and/or (ii) going into the CH_3 radicals as a combination of rotational, vibrational, and translational energy. A two-photon process that would ionize Zn (9.39 eV) is unlikely. The lowest-lying transitions of Zn II would be seen at 6.12 eV (2026 Å, 49 354 cm^{-1}) and/or 6.01 eV (2063 Å, 48 481 cm^{-1}). We did not observe any of the Zn II transitions in this region.

If the excess energy of the first photon went into exciting Zn, the lowest-lying energy level is the $4p$ ($^3P_1$) state at 4.00 eV (32 311 cm^{-1}).[22] The excess energy of ~2.59 eV (20 890 cm^{-1}) is not enough to excite Zn to a higher energy level, as is shown schematically in Fig. 13. This implies that the energy must go into the CH_3 radical. The amount of energy acquired by the methyl radicals upon photodissociation from DMCd and DMZn has been explored by several groups.[46–48] It was found that the υ_2 and υ_3 modes were populated. The translational energy of the CH_3 radicals was found to be only a fraction of the excess energy in the 193 nm dissociation of DMCd.[47] This can account for ~1.70 eV of the ~2.59 eV remaining from the first ArF photon, with the rest of the energy going into another mode, or into further translational energy of the methyl radical.

The amount of energy required to make CH* from CH_3 radicals is 12.07 eV. Ye, Suto, and Lee[49] studied the 193 nm dissociation of methyl radicals and proposed that CH_3 dissociates into CH_2^*, which then absorbs another ArF photon to make CH*. The CH_2 (methylene) radical has two states, a (linear) triplet ground state and a (bent) singlet excited state.[50] A likely possibility for the dissociation of CH_3 is the creation of excited singlet CH_2. Braun and co-workers[45] have shown that the singlet state rather than the triplet state is the major product in the photolysis of ketene and diazomethane. The separation between the triplet and singlet levels is not clear,[51] but is on the order of 0.5 eV, and the absorption of another ArF photon by CH_3 would create excited methylene and leave an excess energy around 1.0 eV to be distributed. The excited singlet CH_2

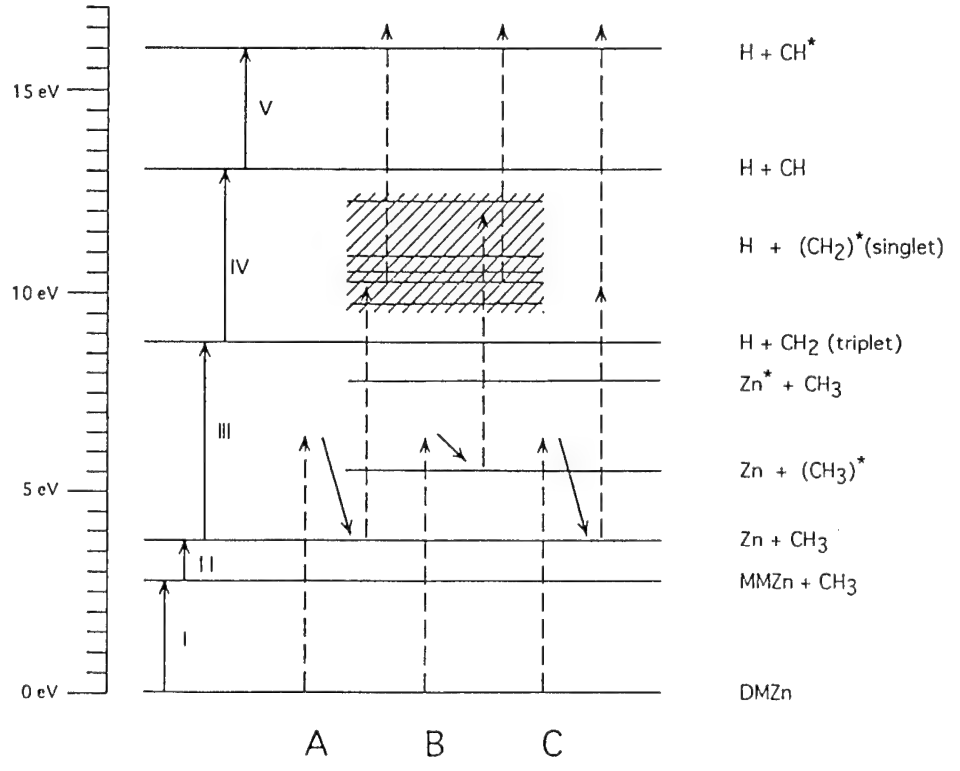

FIG. 13. Schematic of the energies involved in the ArF dissociation of DMZn. The Roman numerals correspond with the reactions listed in Table II. The solid arrows indicate the known dissociation energies, while the dashed arrows represent the absorption of an ArF laser photon (6.42 eV). The hashed area represents the many-line spectrum of the singlet methylene radical, which contains several broad bands. There are three possible reaction pathways shown in the figure for the dissociation process. The first possibility, labeled A, is the stepwise absorption of three photons, with the intermediates being Zn, CH_3, $(CH_2)^*$, and CH*. The second possible reaction pathway, (B) is similar to the first except that excited (as opposed to ground-state) methyl radicals are among the intermediates. The last pathway (C), involves the creation of $Zn+CH_3$, and then the simultaneous absorption of two photons, thus bypassing the creation of the $(CH_2)^*$ intermediate.

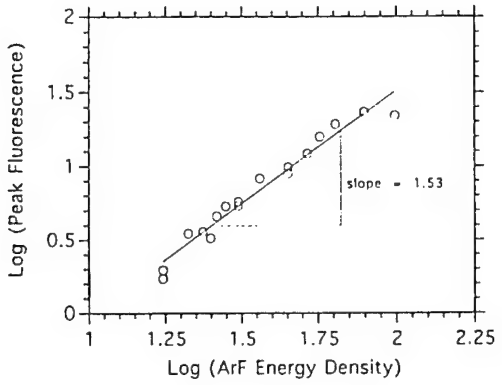

FIG. 14. log/log plot of CH* emission intensity vs ArF energy. The plot is a combination of points taken from two different experiments. The slope of the line is $n=1.55$. The number of photons it takes to create CH* is at least three, but due to saturation effects, the intermediate levels in the formation of CH are depopulated faster than the upper state of CH is populated, thus resulting in a slope $n<3$.

could then absorb another photon, which would create CH*. Another process that could take place involves the simultaneous absorption of two photons by the CH_3 radical. For two ArF photons (12.84 eV), there is enough energy to create CH* from CH_3 directly with 0.77 eV in excess, as shown in process C in Fig. 13. However, this dissociation channel is more energetic than the ionization channel (9.84 eV), and Ye and co-workers indicate that the ionization channel dominates. The dissociation of methyl radicals would seem to favor creation of the excited singlet-state methylene radical $(CH_2)^*$, which then would absorb another ArF photon to create CH*, leaving excess energy for vibrational-rotational-translational modes to be excited.

In a high-energy-density system, absorptions of multiple photons can occur, as is seen in Fig. 13. When the excitation intensity is below the saturation point of a system, the process should exhibit an integral slope between the log of the emission intensity and the log of the excitation intensity:

$$\log(I_{\text{emission}}) = n \log[(h\nu)/t],$$

as has been shown in the dissociation of DMCd at 193 nm.[52] However, when the excitation intensity is in the saturation regime of the system, the slope is no longer integral, but depends on the rates of population and depopulation of the levels involved, the energy fluence, the absorption cross sections of the intermediates, and lifetimes of their states. In Fig. 14, the log/log plot of I_{emission} vs ArF energy for the CH* state has a slope of $n=1.5$. There are at least four processes needed to create CH as shown in Fig. 13, and the population of the upper CH state (and thus the intensity of the emission) may be competing with the collisional or radiative depopulation of one of the intermediate steps. A high fluence of the excitation source may also be affecting the upper state by totally depopulating one of the lower levels. The system which produces CH* is likely in saturation at the energy densities shown in the figure. Similarly, the log/log plots of the Zn and methyl radical concentrations versus ArF energy have slopes ranging from $n=0.3$ to $n=0.6$. If one assumes that the process to make Zn and methyl radicals is a one-photon process, this indicates that both the one-photon and multiple-photon processes are influenced by saturation effects.

The dissociation of DMZn by an ArF laser can be accounted for energetically with three photons, as is seen in Table II. The detected photoproducts are Zn, CH_3, and CH*, with the assumption of intermediate, short-lived ($\leqslant$50 ns) molecules CH_3Zn and $(CH_2)^*$. While other species may be formed in such a high-energy-density system,[53] it is likely that the radicals mentioned above are the only ones present in significant concentrations.

VI. CONCLUSIONS

We have demonstrated a tabletop UV-VUV absorption experiment that is versatile and inexpensive. Although this system is constructed separate from the growth chamber, the system could be easily integrated into an *in situ* growth monitoring technique. The system we have demonstrated can detect concentrations of the photoproducts in a non-invasive manner, thus allowing direct monitoring of deposition concentrations during growth, with a time resolution to within 50 ns of the dissociation.

We have detected both Zn atoms and CH_3 radicals in absorption and quantified their concentrations. We have also detected CH* which is produced in the photodissociation process, and argued that the input energy of the system is accounted for, meaning that the CH* is most likely the only long-lived ($\geqslant$50 ns) excited radical being formed. The Zn is formed in its ground state and remains unreactive for at least several milliseconds. As the Zn concentration does not change, any intermediate compounds that would scavenge it are likely to be negligible. The methyl radicals combine to form ethane and are transported away from the dissociation region, and thus are not being incorporated into the ZnSe films. The CH radicals relax to their ground state within 300 ns and likely react with H_2 to form CH_3. Due to the expected low efficiency of the process to make CH* and its high reactivity with hydrogen, it is likely that these radicals do not effect the films. Thus, the use of a high-energy-density system in the dissociation of DMZn is beneficial to the growth process, and there are no indications that such a system produces any reasonable channels for carbon contamination.

ACKNOWLEDGMENTS

The authors would like to thank Dr. Robert Curl and Dr. Roland Sauerbrey for valuable consultations during the work. Assistance was also provided by Dr. Frank Tittel and Dr. Paul Gillespie. Financial support was provided by Dr. Skip Porter of the Houston Advanced Research Center (HARC) and the Advantest Corporation. This work was performed under DARPA Grant No. N00014-89-J-3122.

[1] H. Jeon, J. Ding, A. V. Nurmikko, W. Xie, D. C. Grillo, M. Kobayashi, R. L. Gunshor, G. C. Hua, and N. Otsuka, Appl. Phys. Lett. 60, 2045 (1992).

[2] J. M. DePuydt, M. A. Haase, J. Qiu, and H. Cheng, J. Cryst. Growth **117**, 1078 (1992).
[3] T. Butkhuzi, A. N. Georgobiani, B. T. Eltazarov, T. G. Khulordava, and M. B. Kotljarevsky, J. Cryst. Growth **117**, 1055 (1992).
[4] J. Ren, K. A. Bowers, B. Sneed, F. E. Reed, J. W. Cook, and J. F. Schetzina, J. Cryst. Growth **111**, 829 (1991).
[5] L. Wei, Y. K. Cho, and C. Dosho, Jpn. J. Appl. Phys. I **30**, 2442 (1991).
[6] S. Fujita, Y. Matsuda, and A. Sasaki, J. Cryst. Growth **68**, 231 (1984).
[7] B. Cockayne, P. J. Wright, M. S. Skolnick, A. D. Pitt, J. O. Williams, and T. L. Ng, J. Cryst. Growth **72**, 17 (1985).
[8] G. B. Shinn, P. M. Gillespie, W. L. Wilson, and W. M. Duncan, Appl. Phys. Lett. **54**, 2440 (1989).
[9] P. M. Gillespie, Ph.D. thesis, Rice University, 1992.
[10] R. L. Jackson, Chem. Phys. Lett. **174**, 53 (1990).
[11] H. Okabe, *Photochemistry of Small Molecules* (Wiley, New York, 1978).
[12] P. Bender, Phys. Rev. **36**, 1543 (1930).
[13] H. Habeeb, D. J. LeRoy, and E. W. Steacie, J. Chem. Phys. **10**, 261 (1942).
[14] M. A. Rueter and J. M. Vohs, Surf. Sci. **268**, 217 (1992).
[15] K. P. Giapis, K. F. Jensen, J. E. Potts, and S. J. Pachuta, Appl. Phys. Lett. **55**, 463 (1989).
[16] R. Larciprete and E. Borsella, Chem. Phys. Lett. **147**, 161 (1988).
[17] E. S. J. Robles, A. M. Ellis, and T. A. Miller, Chem. Phys. Lett. **178**, 185 (1991).
[18] P. Laporte, N. Damany, and H. Damany, Opt. Lett. **12**, 987 (1987).
[19] S. Kubodera, L. Frey, P. J. Wisoff, and R. Sauerbrey, Opt. Lett. **13**, 446 (1988).
[20] P. S. Millar, T. Peterson, G. Warwar, P. J. Wisoff, and R. Sauerbrey, Opt. Lett. **14**, 171 (1989).
[21] C. J. Chen and R. M. Osgood, J. Chem. Phys. **81**, 327 (1984).
[22] C. E. Moore, *Atomic Energy Levels NSRDS-NBS 35* (National Bureau of Standards, Washington, DC, 1971), p. 124.
[23] G. Herzberg, *Molecular Spectra and Molecular Structure III. Electronic Spectra of Polyatomic Molecules* (Van Nostrand, New York, 1966).
[24] Y. Fujita, S. Fujii, and T. Iuchi, J. Vac. Sci. Technol. A **7**, 276 (1989).
[25] T. Ibuki, A. Hiraya, and K. Shobatake, J. Chem. Phys. **92**, 2797 (1990).
[26] R. D. Anderson and H. A. Taylor, J. Phys. Chem. **56**, 498 (1952).
[27] A. M. Bass and A. H. Laufer, Int. J. Chem. Kin. **5**, 1053 (1973).
[28] J. I. Steinfeld, *Chemical Kinetics and Dynamics* (Prentice-Hall, Englewood Cliffs, NJ, 1989).
[29] A. Callear and H. E. van den Berg, Chem. Phys. Lett. **5**, 23 (1970).
[30] W. Tsang and R. F. Hampson, J. Phys. Chem. Ref. Data **15**, 1087 (1986).
[31] A. Corney, *Atomic and Laser Spectroscopy* (Clarendon, Oxford, 1988).
[32] C. H. Corliss and W. R. Bozman, *Experimental Transition Probabilities for Spectral Lines of Seventy Elements* (National Bureau of Standards, Washington, DC, 1962), Vol. 53, p. 540.
[33] R. H. Barnes, C. E. Moeller, J. F. Kircher, and C. M. Verber, Appl. Opt. **12**, 2531 (1973).
[34] M. Clerc and M. Schmidt, Faraday Discuss. Chem. Soc. **53**, 217 (1972).
[35] C. F. Yu, F. Youngs, K. Tsukiyama, R. Bersohn, and J. Preses, J. Chem. Phys. **85**, 1382 (1986).
[36] P. J. Young, R. K. Gosavi, J. Connor, O. P. Strausz, and H. E. Gunning, J. Chem. Phys. **58**, 5280 (1973).
[37] R. L. Jackson, J. Chem. Phys. **92**, 807 (1990).
[38] W. Kedzierski, J. Supronowicz, J. B. Atkinson, and L. Krause, Can. J. Phys. **68**, 526 (1990).
[39] W. H. Breckenridge and J. H. Wang, Chem. Phys. Lett. **123**, 17 (1986).
[40] G. Herzberg, *Molecular Spectra and Molecular Structure I. Spectra of Diatomic Molecules* (Krieger, Malabar, FL, 1989).
[41] J. Berkowitz, *Photoabsorption, Photoionization, and Photoelectron Spectroscopy* (Academic, New York, 1979).
[42] S. Fujita, S. Maruo, H. Ishio, P. Murawala, and S. Fujita, J. Cryst. Growth **107**, 644 (1991).
[43] S. Fujita, S. Hirata, and S. Fujita, Jpn. J. Appl. Phys. **30**, L507 (1991).
[44] K. P. Giapis, K. F. Jensen, J. E. Potts, and S. J. Pachuta, J. Electron. Mater. **19**, 453 (1990).
[45] W. Braun, A. M. Bass, and M. Pilling, J. Chem. Phys. **52**, 5131 (1970).
[46] S. L. Baughcum and S. R. Leone, Chem. Phys. Lett. **89**, 183 (1982).
[47] J. O. Chu, G. W. Flynn, C. J. Chen, and R. M. Osgood, Chem. Phys. Lett. **119**, 206 (1985).
[48] H. S. Gutowsky, J. Am. Chem. Soc. **71**, 3194 (1949).
[49] C. Ye, M. Suto, and L. C. Lee, J. Chem. Phys. **89**, 2797 (1988).
[50] G. Herzberg, Proc. R. Soc. London Ser. A **262**, 291 (1961).
[51] J. Danon, S. V. Filseth, D. Feldmann, H. Zacharias, C. H. Dugan, and K. H. Welge, Chem. Phys. **29**, 345 (1978).
[52] M. Suto, C. Ye, and L. C. Lee, J. Chem. Phys. **89**, 160 (1988).
[53] V. M. Donnelly, M. Geva, J. Long, and R. F. Karlicek, Appl. Phys. Lett. **44**, 951 (1984).
[54] R. L. Jackson, Chem. Phys. Lett. **163**, 315 (1989).

Journal of Electronic Materials, Vol. 23, No. 2, 1994

Photodissociation Dynamics of DMZn at 193 nm: Implications for the Growth of ZnSe Films by Laser-Assisted Metalorganic Chemical Vapor Deposition

JOSEPH A. ELIAS, PETER J. WISOFF,* and WILLIAM L. WILSON, JR.

Department of Electrical and Computer Engineering, Rice University, Houston, TX 77251

The chemical dynamics of the photodissociation of dimethylzinc (DMZn) have been investigated using VUV absorption spectroscopy. An ArF excimer laser (193 nm) was used to photodissociate DMZn in a hydrogen atmosphere. A broadband pulsed VUV plasma light source was used to obtain absorption profiles of the resulting photoproducts as a function of time after the dissociation pulse. The time-resolved absorption profiles indicate that ground state Zn atoms remain unreacted for at least several milliseconds, while the only other species detected in absorption, methyl radicals, disappear within a few hundred microseconds. There was no indication of monomethylzinc (MMZn) or zinc hydride (ZnH) formation. The methyl radical decay followed a second-order reaction rate, indicating that the main by-product is ethane. This conclusion is supported by mass spectrometer data. Fluorescence from CH* radicals was also detected after the ArF laser pulse. Due to the high reactivity of CH radicals, it is likely that they combine with hydrogen to form methyl radicals within several microseconds. A model for the methyl radical diffusion to the growth surface is discussed. The possible carbon containing intermediates (MMZn, CH_3, CH) are unlikely to reach the growth surface in significant concentrations. Thus, carbon incorporation should be minimal using laser-assisted metalorganic chemical vapor deposition growth technique.

Key words: Dimethylzinc, photodissociate, methyl radical absorption, zinc absorption, ZnSe

INTRODUCTION

Wide band gap semiconductors such as ZnSe are promising optoelectronic materials for blue lasers,[1] light emitting diodes,[2] and optical switches,[3] as well as for use in GaAs-based metal insulator semiconductor field effect transistors.[4] The quality of ZnSe thin films grown by metalorganic chemical vapor depositon (MOCVD) has been hampered by defects,[5] and it has been shown that lower growth temperatures reduce their density.[6]

Our group has been investigating the epitaxy of ZnSe films grown at reduced substrate temperatures by utilizing a laser-assisted metalorganic chemical vapor deposition (LAMOCVD) process.[7] In this technique, an ArF excimer laser is focused parallel to a GaAs substrate (as is shown in Fig. 1) and is used to photodissociate the source gases (DMZn, DESe), substituting in part for the usual thermal energy which is used in conventional MOCVD systems. With the LAMOCVD growth method, excellent quality epitaxial ZnSe films are routinely achieved. More recently, p-type films have been grown using NH_3 as the dopant source. Figure 2 depicts 12K photoluminescence spectra for both undoped and nitrogen-doped films grown by this process. Films treated by post-growth annealing have recently shown active hole concentrations of $\sim 1 \times 10^{18}$ cm^{-3}. While this LAMOCVD method yields good quality ZnSe films, the fundamental chemistry of the dissociation process is not well understood. Depending on the UV source, the photodissociation of DMZn, DESe, and NH_3 results in intermediate compounds such as

(Received March 25, 1993; revised June 17, 1993)

*Present address: NASA, JSC, Houston, TX 77058

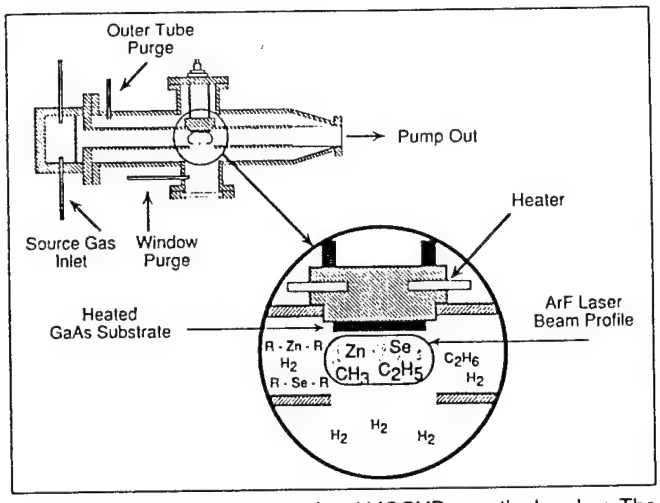

Fig. 1. Side view of the laser-assisted MOCVD growth chamber. The metalorganics flow left to right, and they are photo-dissociated below the GaAs substrate by an ArF laser beam which is going into and out of the page. The center of the beam profile is about 50 mm from the substrate (not drawn to scale). Not shown are the windows through which the beam is directed.

MMZn[8] and NH_2.[9] The role of these intermediate products in the growth process, however, has not been investigated in detail to date. However, in a similar system, the photodissociation of molecules such as DMCd and DMTe has been studied, and a model for this process has been developed[10] for HgCdTe growth.

Also of concern when using MOCVD for the growth of semiconductor films is the incorporation of carbon from the organic radicals into the film during growth.[11-13] Carbon is known to be electrically active and can be detrimental to film quality. Using laser radiation to photodissociate the metal organic precursors near the growth surface may help eliminate this problem. The present work concentrates on the 193 nm photodissociation dynamics of DMZn in a hydrogen atmosphere, and its implications for the growth of ZnSe films.

Metalorganics inherently have the potential for delivering unwanted carbon-containing molecules to the growth surface. The transport of monomethyl metal radicals, methyl radicals, and/or other carbon species to the substrate can result in subsequent incorporation of carbon into the film. Besides carbon contamination, the transport of metal atoms (Zn, Se) to the surface may be retarded through the formation of intermediate molecules such as ZnH[14] or H_2Se. The possible formation of intermediate compounds and the role these may play in the growth process need to be explored in order to improve the overall control and quality of LAMOCVD ZnSe films.

EXPERIMENT

Dissociation-Probe System

The products and rate reactions resulting from the photodissociation of dimethylzinc after irradiation from an ArF excimer laser were studied in a specially constructed multi-chamber reaction cell. As shown in Fig. 3, DMZn and hydrogen were allowed to flow through the central portion of the apparatus. An ArF

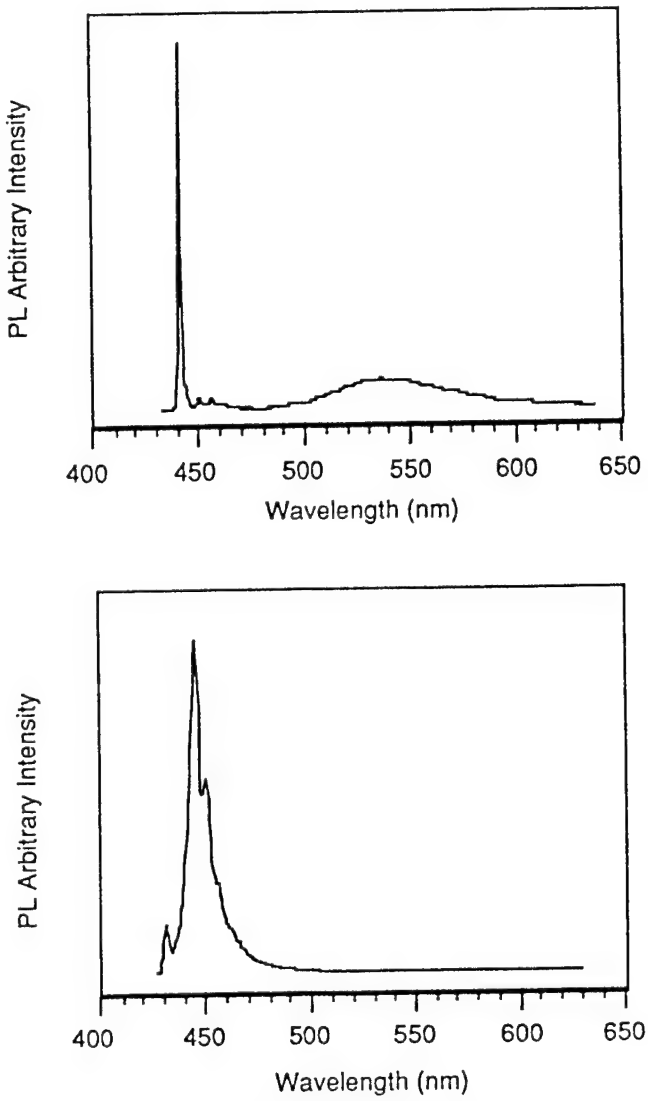

Fig. 2. Photoluminescence spectra taken at 12K for both (a) undoped and (b) nitrogen-doped ZnSe films. The free exciton peak at 442 nm is evident in (a) which is an indication of good crystallinity, along with a slight broadband feature due to dislocations resulting from the lattice mismatch between ZnSe and GaAs. The acceptor-bound exciton peak at 444 nm in (b) is an indication of nitrogen incorporation in the films. Recent C-V profiling has indicated this dopant source incorporates ~1 e18 cm^{-3} active holes in the films.

excimer laser was focused through the cell, directed to one side of the entrance slits of a vacuum UV spectrometer. The 193 nm photons from this excimer laser source were used to photodissociate the DMZn. Following the ArF photodissociating pulse, an Nd:YAG laser, tightly focused into a second cell which contained approximately 200 Torr of argon, was triggered. The energy of the focused Nd:YAG laser (0.8 J) was sufficient to cause breakdown of the argon gas, creating an intense plasma emission which extended in wavelength from the visible through the vacuum ultraviolet. The emission from this plasma breakdown was then used to back-light the dissociation region. By scanning the spectrometer, absorption features due to products of the photodissociation process were detected and analyzed. The plasma

emission was temporally short (~200 ns) which meant that as the delay of the Nd:YAG laser was varied with respect to dissociating ArF laser pulse, the kinetics of the formation and decay of the various photoproducts could be determined with good temporal resolution.

The ArF laser beam was rectangular in cross section, with an area of about 0.3 cm^2. The energy density was varied from 250 mJ/cm^2 to 20 mJ/cm^2. The signal which passed through the spectrometer was detected with a solar-blind photomultiplier tube, and then processed with a boxcar integrator and microcomputer. The relative timing between the ArF laser photodissociation pulse, the Nd:YAG laser pulse, the argon emission, and the boxcar gate are shown in Fig. 4. Both the Nd:YAG pulse and the boxcar gate position were varied from about 50 ns after the dissociating pulse (limited by optical noise resulting from stray ArF laser radiation entering into the spectrometer) to about 2 ms after the pulse (limited by diffusion of undissociated DMZn into the reaction region, and subsequent loss of optical signal).

Figure 5 shows a typical spectrum which was observed both with and without DMZn passing through the absorption cell. For these scans, no ArF photodissociation pulse was used. This spectrum is a mixture of continuum (free-free transitions in the plasma) and line emission (bound-free transitions) resulting from excited Ar II and Ar III. The scan was limited on the short wavelength side ($\lambda \sim 1150$Å) by the transmission characteristics of the MgF_2 windows used to separate the various regions of the experiment. The scan was extended only to 2500Å on the long wavelength side, as this was the region in which the anticipated photoproducts have absorption transitions.

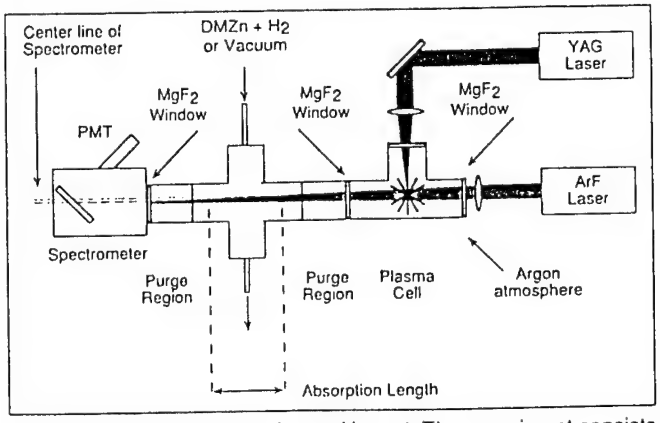

Fig. 3. Top view of the experimental layout. The experiment consists of a photodissociation laser (ArF), a laser (Nd:YAG) to create the plasma probe source, a 0.25 m spectrometer, a solar-blind PMT, a gated boxcar integrator, a timing control generator, an oscilloscope, and a microcomputer. The source gases flow through the center region and hydrogen purges are used to limit unwanted metal deposition on the windows. The absorption cell and plasma cell are separated by a MgF_2 window which allows wavelengths longer than λ~1150Å to be transmitted. The absorption cell is operated at a typical pressure of 25 Torr of DMZn + H_2; the plasma cell operates at several hundred Torr of argon, and the spectrometer is kept at vacuum. The ArF laser beam is directed slightly off axis so as to prevent 193 nm radiation from entering into the spectrometer.

Absorption Experiments

When DMZn was allowed to flow through the absorption cell, the second spectrum shown in Fig. 5 resulted. Absorption bands centered around 2000Å and in the short-wavelength regime (centered about 1500Å) are clearly visible. The ArF excimer (λ = 1933Å) photodissociates the molecule due to its relatively large absorption cross section around 2000Å.[15]

A number of different scans, taken at various times

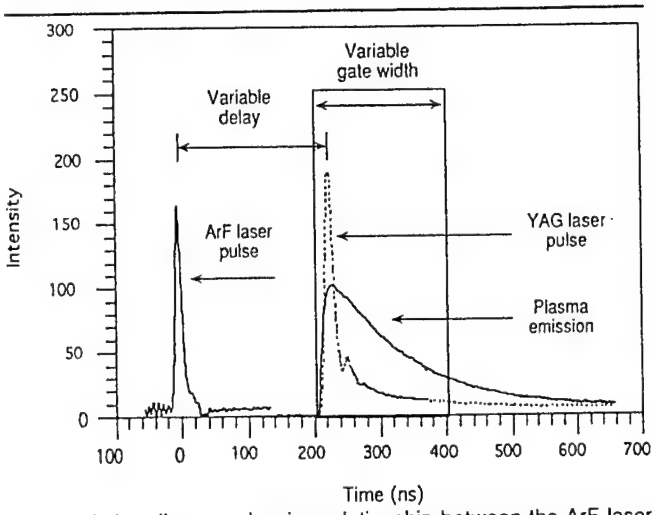

Fig. 4. Timing diagram showing relationship between the ArF laser pulse, the Nd:YAG laser pulse, the plasma emission, and the boxcar gate. The timing between the ArF laser pulse and the plasma emission can be varied from zero delay to several seconds delay, if necessary. Due to flow of undissociated DMZn into the optical column, the upper limit on the time resolution is ~2 ms. The lower resolution of the timing is limited by the jitter of the ArF laser (± 25 ns). It is found that the best repeatability of the data is obtained with 200 ns gate widths. It should be noted that, in the figure, the relative intensities of the ArF laser pulse, the YAG laser pulse, and the plasma emission are not to scale.

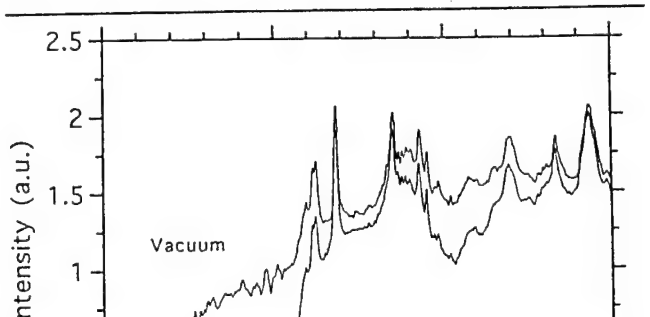

Fig. 5. Typical spectral output of the plasma emission from 1000 to 2500Å. The upper trace is the plasma spectrum detected with vacuum in the absorption cell, and the lower trace is the detected plasma spectrum observed with 40 mTorr of DMZn in the absorption cell. Two broadband absorptions can be seen, one around 2000Å (near the emission wavelength of the ArF laser), and another in the deep VUV from 1200 to 1600Å. The ionized Argon, mainly Ar II and Ar III, create line emission due to bound-bound transitions and a broad continuum which is due mainly to free-free transitions, or bremsstrahlung.

after the ArF photodissociation pulse are shown in Fig. 6. For reference, a vacuum spectrum is shown in the background. Although a H_2 purge was used around both MgF_2 windows in the absorption cell, a slight Zn film was deposited on the windows. As a result, the ArF laser beam was not used during the entire scan. This procedwe can be observed in the various scans shown in Fig. 6 by the near zero signal observed for $\lambda < 2100$Å. While this spectral region was being scanned, the ArF laser beam was blocked by a shutter, and as a result, the DMZn in the cell completely absorbed emission from the argon plasma. When the shutter was opened, a significant fraction of the DMZn in the absorption path was photodissociated, and an increase in the detected emission signal was observed.

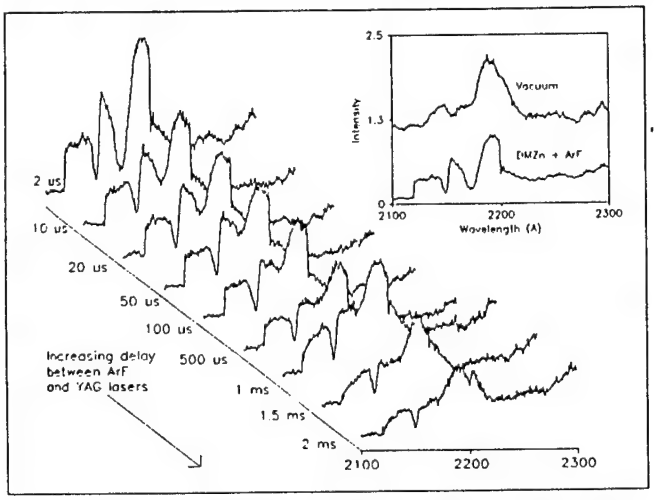

Fig. 6. Variation of absorption profiles at different delay times. A plasma spectra through vacuum and the spectra taken at 2 μs delay is shown for reference in the inset. The CH_3 absorbance decays after several hundred microseconds, while the Zn profile remains constant (the relative depth of the Zn absorption is the same at 2 μs as at 2 ms). The overall signal intensity decreases as undissociated DMZn flows back into the dissociation region. The resolution of the spectrometer for these experiments was 6Å.

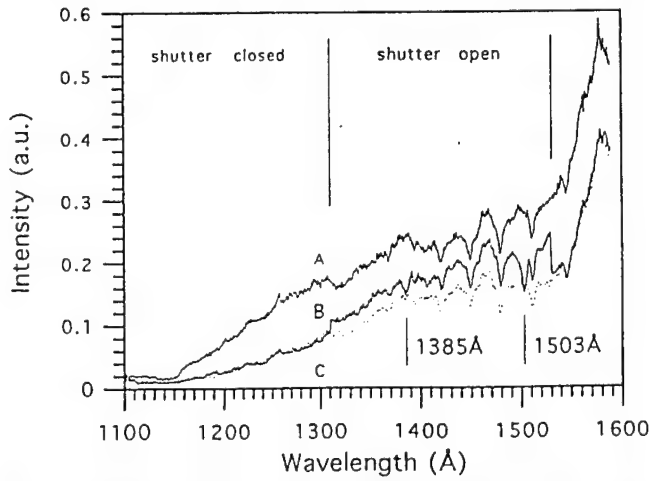

Fig. 7. Absorption features of CH_3 in the deep VUV. Curve A is the plasma spectrum through vacuum; Curve B is the spectrum with DMZn in the reaction region and with the ArF laser shutter opened from ~1310–1530Å; and Curve C is the spectrum detected with DMZn in the reaction region and no irradiation from the ArF laser. The two features are the 1503Å ($C \leftarrow X$) and 1385Å ($\delta_2 - \gamma_2 \leftarrow X$) bands.

Absorption features from only two different species in the spectral range 1150–3500Å could be observed as a result of the photodissociation of DMZn by the ArF excimer laser. One was atomic zinc, which has a ground state absorption ($4^1P_1 \leftarrow 4^1S_0$) at 2139Å and the other was CH_3 for which the 2160Å ($B \leftarrow X$)[16] absorption feature is shown in the figure. As is evident from Fig. 6, the absorption feature at 2160Å associated with the CH_3 radical decays to below the detection limit after a few hundred microseconds, whereas the Zn absorption feature remains more or less constant in time out to well over a millisecond. Two other absorptions bands for CH_3 shown in Fig. 7, the 1503Å ($C \leftarrow X$) and 1385Å ($\delta_2 - \gamma_2 \leftarrow X$)[16] were also observed but had lower signal to noise ratios because of the stronger absorption of the residual DMZn at these wavelengths.

Methyl Radical Concentrations

To determine the density of CH_3 absorbers in the optical column, the time decay of the methyl radical absorption was recorded, and gas kinetics were used to determine the initial concentration of radicals present. The dominant reaction for the removal of CH_3 was found to be the recombination reaction:

$$CH_3 + CH_3 + M \rightarrow C_2H_6 + M. \quad (1)$$

This reaction is second order in CH_3, whereas the reaction to form methane:

$$CH_3 + H_2 \rightarrow CH_4 + H \quad (2)$$

is a first order reaction in CH_3 (see Table I). The methyl radical absorbance decay followed a second order reaction, thus in our system, ethane production was the dominant loss mechanism for CH_3. It has been previously shown[17,18] that ethane is the major product of the recombination of methyl radicals in the photolysis of DMCd.

The decay of the methyl radical absorbance signal at 2160Å vs time is shown in Fig. 8. Attempts at both first order and second order curve fits are also shown in the figure. As is evident, a second order reaction for the decay of CH_3 is a much better fit to the data than a simple exponential (first order) decay. Analysis by mass spectrometry also supports the conclusion that ethane was the major product of this photodissociation process. In Fig. 9, the mass spectra for several species are shown as the ArF excimer laser was switched on and off. In this experiment, DMZn was being transported to the mass spectrometer. Dissociation by the ionization head resulted in the background concentrations of hydrocarbons seen in the figure. The quadrupole detector head was located over a meter away from the photodissociation region. Thus, any transient species (such as CH_3) would have decayed away or recombined before they arrived at the detection system. Ethane, C_2H_6, mainly cracks into C_2H_4 and C_2H_3 in the spectrometer ionizing head. The concentration of mass 28 (C_2H_4) increased significantly when the ArF laser was turned on. The concentration of mass 27 (C_2H_3) and mass 16 (CH_4)

Table I. Reaction for the Removal of CH_3[20]

	Reaction			k (300K) cm³/molecule second	k (673K) cm³/molecule second
I	$CH_3 + H_2$	→	$CH_4 + H$	1.2×10^{-20}	4.7×10^{-16}
II	$CH_3 + H$	→	CH_4	2.0×10^{-10}	1.5×10^{-10}
III	$CH_3 + CH_3 + M$	→	$C_2H_6 + M$	4.4×10^{-11}	2.6×10^{-11}
IV	C_2H_6	→	$CH_3 + CH_3$	5.2×10^{-49}*	7.2×10^{-13}*

*Units for unimolecular reaction rate coefficient: $cm^6/molecules^2\ sec^2$.

increased only slightly, while the partial pressure of mass 15 (CH_3) (a cracking product of CH_4) does not change. Since the only significant change observed when the ArF laser was turned on was an increase in C_2H_4, we infer that ethane (C_2H_6) was the primary hydrocarbon product resulting from the photodissociation of DMZn.

In order to determine the density of absorbing CH_3 radicals N(t), the kinetic equations for a second-order reaction were used:[19]

$$\frac{dN(t)}{dt} = -2k\,N^2(t) \qquad (3)$$

where k is the rate reaction constant with a value of $k = 4.4 \times 10^{-11}$ molecules^{-1} cm^3 sec^{-1} at room temperature.[20]

Rearranging and integrating:

$$N(t) = \frac{N_0}{N_0 2k\,t + 1} \qquad (4)$$

From Beer's Law, the absorbance (A):

$$A(t) = \ln\frac{I_0}{I(t)} = N(t)\sigma L \qquad (5)$$

where $\frac{I_0}{I(t)}$ is the ratio of the intensity without and with the absorbing species at any given time.

Combining Eqs. (4) and (5):

$$A(t) = N(t)\sigma L = \frac{A(0)}{A(0)K\,t + 1} \qquad (6)$$

where $K = 2k/\sigma L$ and $A(0) = N_0\,\sigma L$.

Equation (6) was then used to fit the CH_3 absorbance signal decay. From the curve fit, the constant K was determined. To determine N_0, the term (σ L) was found from the relations in Eq. (6):

$$\sigma L = \frac{2k}{K} \qquad \text{and} \qquad N_0 = \frac{A(0)}{\sigma L}$$

As was also observed by Callear[21] and Bass,[18] the methyl radical absorption did not peak until several microseconds after the dissociation, as shown in the insert to Fig. 8. This was attributed to methyl radicals initially appearing in an excited state, which were then collisionally relaxed to the ground state. For the recombination rate analysis, the production of methyl radicals ceases 2 μs after the ArF pulse, and the curve fit to the decay begins at that point.

For the data shown in Fig. 8, K was found to be equal to 0.856 μs^{-1}. Substituting back into Eq. (6), the initial concentration of CH_3 was $N_0 = 1.28 \times 10^{15}$ cm^{-3}. This is compared with the known initial concentration of DMZn, $N_{DMZn} = 1.30 \times 10^{15}$ cm^{-3}, calculated from flow rates and pressures of the gas delivery system.

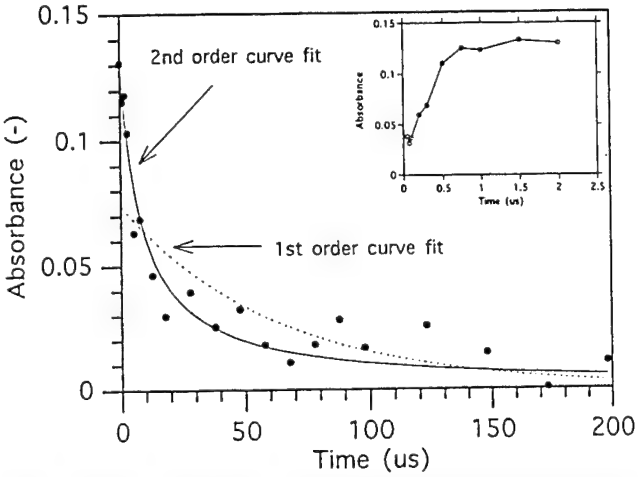

Fig. 8. Decay of the CH_3 ($B \leftarrow X$) absorbance in time. The dotted line is an attempt at a simple first order decay, whereas the solid curve represents a second order decay fit to the data.

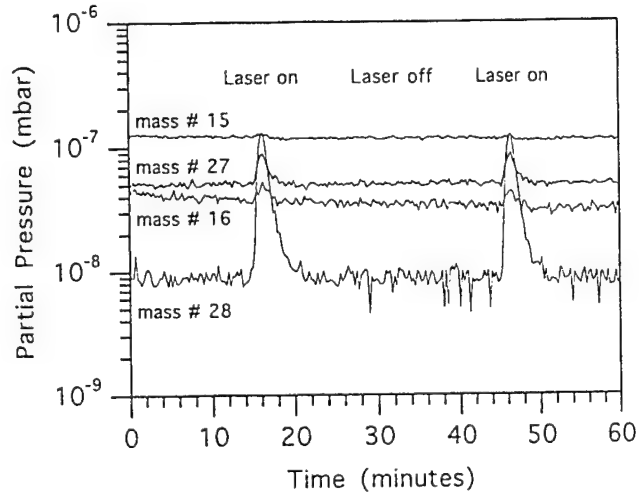

Fig. 9. Mass spectra of the by-products of the photodissociation process. Mass 15 (CH_3), 16 (CH_4), 27 (C_2H_3), and 28 (C_2H_4) were recorded with the ArF laser on and off. The change in concentration is greatest for mass 28, and while there is little change for mass 16, and no change for mass 15. This is a good indication that ethane (C_2H_6) is the primary product rather than ethane (CH_4). The background concentration of the hydrocarbons is due to the dissociation of the DMZn molecule by the ionizer head of the quadrupole.

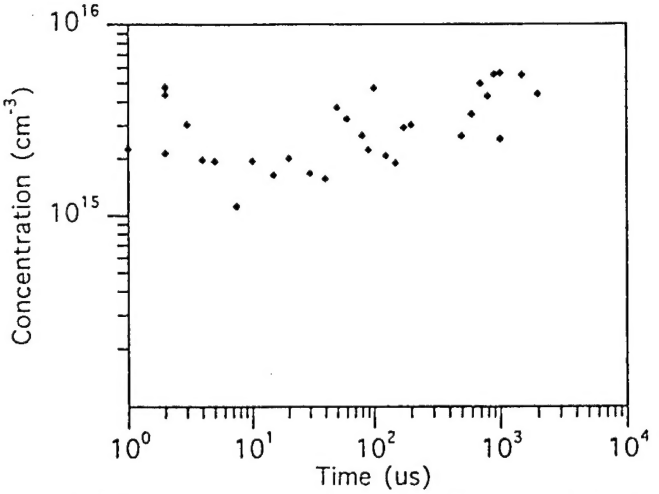

Fig. 10. Observed Zn concentration vs time. The concentration is calculated from the equivalent width of Zn, and a "curve of growth." The calculated number of Zn atoms agrees well with the initial DMZn concentration. The relatively constant concentration shows that the formation of intermediate compounds such as ZnH do not scavenge appreciable numbers of Zn atoms.

The pressure calculations were confirmed by the good agreement with other groups[15,22] on the DMZn cross section measurements. Both the reaction kinetics and the change in the overall broadband DMZn absorption indicated that, at the energy densities used in these experiments, approximately half of the DMZn was being dissociated, since two CH_3 radicals would be expected from each dissociated DMZn molecule.

The formation of ethane from the recombination of methyl radicals has important implications on the incorporation of carbon in the films. Ethane does not absorb 193 nm radiation,[23] thus one would not expect the ethane that had been formed by the recombination of methyl radicals to be dissociated by the next ArF pulse. Giapis[13] showed with secondary ion mass spectroscopy and photoluminescence (PL) data analysis that carbon can be incorporated into MOCVD grown ZnSe films from the metalorganic precursors. The carbon contamination was correlated with the PL peak I_c located at 2.7920 eV. The PL of ZnSe films grown by our LAMOCVD method show no evidence of this PL emission, which is one indication that C contamination is not present in significant concentrations in the films.

Zinc Absorption

In order to extract the concentration of Zn atoms in the optical column, the equivalent width of the Zn resonant absorption line is analyzed. Following Corney[24] and Thorne,[25] one can show for optically thick absorbing columns dominated by pressure broadening, the number of absorbing atoms N is given by:

$$N = \frac{(W_\omega)^2 \varepsilon_0 mc}{\pi e^2 f_{ik} L \Gamma} \qquad (7)$$

where L = absorption length (m), Γ = Lorentzian linewidth (s^{-1}), f_{ik} = absorption oscillator strength, and W_ω = equivalent width (s^{-1}).

However, when the gas is not in a high pressure regime, the line shape is described by a combination of Gaussian (Doppler broadened) and Lorentzian (pressure broadened) linewidths. In this case, in order to determine the number of absorbers, a "curve of growth" is used.[24] Using the oscillator strength of the zinc absorption transition, gf = 1.3,[26] the Doppler broadening has a value of Δ = 2.15 GHz. The pressure broadening comes from natural (Γ_1 = 118 MHz) and hydrogen-pressure broadening (Γ_2 = 33 MHz). Taking their ratio and applying it to the curve of growth gives a Zn concentration of a few 10^{15} cm^{-3}. Although there is some scatter to the data, the observed Zn concentration shows no trend either up or down over a time regime extending from 100 ns to 2 ms after the dissociation pulse as shown in Fig. 10. This indicates that the Zn atoms were not reacting with any other species to form intermediate compounds over this time period. Any intermediate compound which would consume Zn (such as ZnH) would have to be formed within the first 50 ns or have a lifetime longer than several milliseconds.

Other possible intermediate compounds that can be formed from the photodissociation of DMZn are ZnH and MMZn. In the present work, there are no indications of the formation of either of these intermediate compounds. Others have explored the MMZn radical by absorption[27] and laser induced fluorescence.[8] For DMZn photodissociation, it has been established that the emission at λ = 4128Å and λ = 4176Å is due to the A→X band of MMZn. There is no detected emission in the present experiments from these transitions or any of the other known transitions of MMZn,[27] λ = 2671Å and λ = 2739Å. A set of experiments was also carried out to look for the monomethyl fragment in absorption at these wavelengths and no signal was found. The photosensitized reaction to form ZnH {$Zn(4^3P_1) + H_2 \rightarrow ZnH$} has also been explored.[28,29] No signal was detected in this work in the regions identified for ZnH emission.[28] The lifetime of ZnH has been shown to be approximately 10 µs.[28] Any ZnH that is formed would decay to ground state Zn and hydrogen, and a change in the Zn concentration would be observed on a 10 µs time scale. As discussed previously, the calculated Zn concentration is within a factor of three of the expected density, and no change in the Zn concentration was observed over several milliseconds. Thus, it is unlikely that any photosensitized reaction to form ZnH consumes an appreciable number of Zn atoms. Further, it can be inferred that nearly all of the Zn is being formed in a ground state, and that *if* there is the formation of another state of Zn, it does not have an appreciable effect on the growth process.

Modeling of Zn and Methyl Concentrations

The modeling of the diffusion of methyl radicals to the growth surface can lend insight into the dynamics of the LAMOCVD technique. Figure 11 indicates the concentration of methyl radicals as a function of time and distance from the center of the ArF laser beam profile. The model is based on the diffusion equation:[30]

$$\frac{dN_1}{dt} = D_{12}\frac{\partial^2 N_1}{\partial x^2} \quad (8)$$

where the diffusion coefficient for species N_1 in an ambient of species N_2 is given by:

$$D_{12} = \frac{N_1\lambda_2\upsilon_2 + N_2\lambda_1\upsilon_1}{3(N_1 + N_2)} \quad (9)$$

Here υ represents the average thermal velocity of each species, and λ is the mean free path, given by:

$$\lambda_1 = \frac{1}{\sqrt{2}\pi N_1 d_1^2 + \sqrt{1+\frac{m_1}{m_2}}\pi N_2 d_{12}^2} \quad (10)$$

where m_1 and m_2 are the masses of species 1 and 2, respectively, and d_1 is the diameter of species 1 and d_{12} is the average spacing between species 1 and 2.

This simple diffusion approach lends insight into the temporal relation of the photoproducts, and can be iteratively solved at discrete points in time. Figure 11 shows diffusion of Zn and CH_3 for times on the order of several milliseconds after the dissociation pulse. The x-axis is the distance from the center of the ArF beam profile. In calculating these profiles, it was assumed that the initial distribution of both Zn and CH_3 had a Gaussian profile, and that this Gaussian shape was preserved throughout the diffusion process.

The results qualitatively indicate the advantage of using laser assistance for growing a semiconductor thin film from metalorganic precursors. Whereas Zn atoms reach the substrate with a significant concentration within several milliseconds after the ArF laser pulse, very few methyl radicals ever reach the growth surface. Growth of ZnSe films by LAMOCVD produces free Zn atoms which then transport to the growth surface while the active carbon-containing compound (methyl radicals) recombines in a region in time and space that renders it unreactive, and hence lowers carbon incorporation in the films.

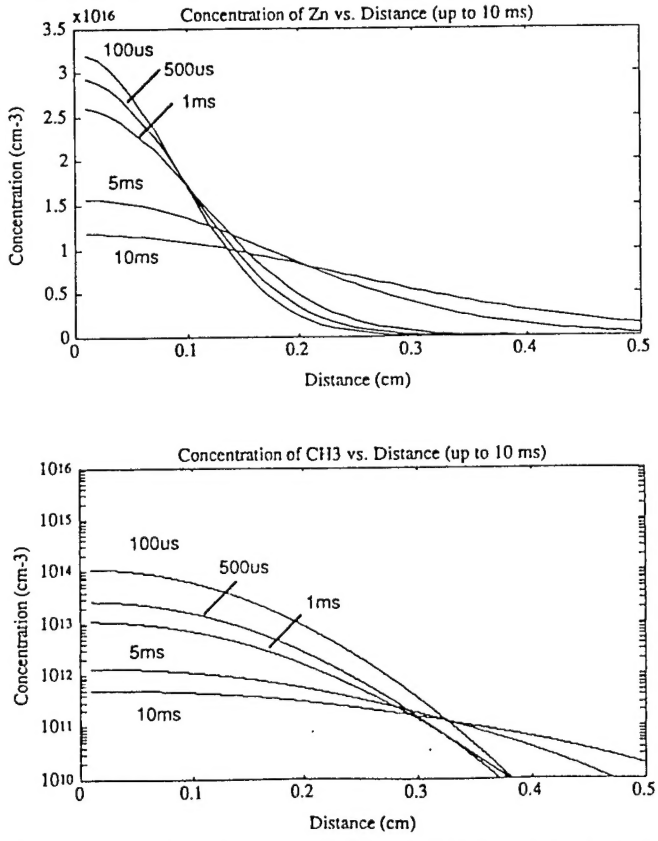

Fig. 11. Model of the diffusion of Zn and CH_3 species. The plot is of the species' concentration vs distance from the center of the ArF laser beam profile, at various times from the trigger of the ArF laser. In the LAMOCVD growth reactor, the substrate is approximately 50 mm from the center of the beam. The methyl radicals recombine during the diffusion, thus they do not reach the substrate in significant concentration.

Fluorescence Experiments

A bright blue emission was observed in the region of photodissociation of DMZn by the 193 nm ArF excimer laser radiation. Spectral analysis of this emission using the spectrometer and a PMT sensitive in the visible indicated a strong emission line at 4315Å. The boxcar gate width was larger than the jitter of the ArF laser. The blue emission, whose spectrum is shown in Fig. 12, is due to the CH ($A\,^2\Delta \rightarrow X\,^2\Pi$) transition.[31] The features of the P, Q, and R branches of the transition are clearly resolved. A plot of the decay of CH* vs time is shown in Fig. 13. Using an exponential curve fit, the upper state lifetime τ of the A state is estimated to be $\tau \sim 80$ ns. This compares with the radiative lifetime $\tau = 580$ ns.[32] The decay of CH* in our system is apparently dominated by collisional de-excitation with H_2.

The results of the fluorescence experiments show

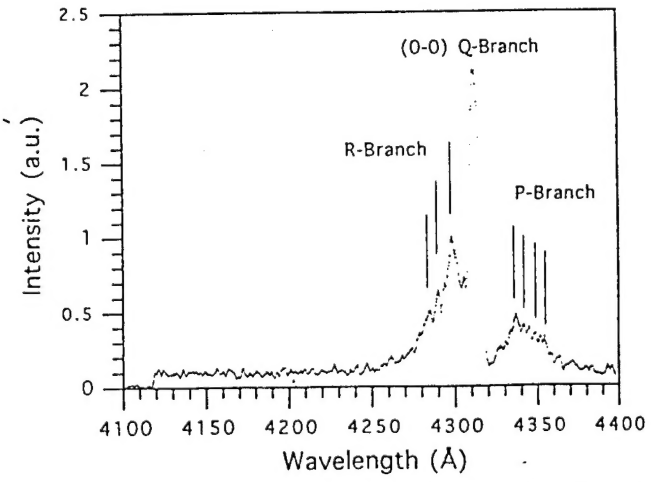

Fig. 12. Emission from the $A \rightarrow X$ transition of the CH radical. The peak at 4315Å is due to the 0-0 Q-branch transition, and the P-branch and R-branch vibrational transitions are also evident. Also of note is the lack of emission at 4128 or 4176Å which are identified with the $A \rightarrow X$ transitions of MMZn. The spectral resolution of the spectrometer for these experiments was 10Å.

that CH* is being produced, but its concentration is not known. The reactivity of CH is substantial. Once the CH* has decayed to its ground state (within 300 ns), it would react very quickly. CH radicals react very efficiently with H_2 in the reaction: $CH + H_2 \rightarrow CH_3$ with $k = 1.00 \times 10^{-12}$ molecules^{-1} cm^3 sec^{-1}.[33] The H_2 concentrations in our experiments were about 1×10^{18} cm^{-3}, thus almost all the CH would react with H_2 within several microseconds. It is unlikely that any unreacted CH radicals would survive long enough to reach the growth surface.

The dissociation of DMZn and the subsequent formation of CH* by an ArF laser can be accounted for energetically with three photons, as is seen in Table II. The detected photoproducts are Zn, CH_3, and CH*, with the assumption of intermediate, short-lived (≤50 ns) molecules CH_3Zn and (CH_2)*. While other species may be formed in such a high energy density system,[34] it is likely that the radicals mentioned above are the only ones present in significant concentrations.

CONCLUSIONS

We have reported on a set of UV-VUV absorption experiments on the photodissociation of DMZn by an ArF excimer laser. We have detected Zn atoms and CH_3 radicals in absorption and quantified their concentrations. We have also detected CH* which is produced in the photodissociation process, and it is likely that CH is the only long-lived (≥50 ns) excited radical being formed. Zinc is formed in its ground state and remains unreacted for at least several milliseconds. The calculated Zn concentration is in good agreement with the initial DMZn concentration, and as the Zn concentration does not change, the formation of any intermediate compounds that would scavenge it are likely to be negligible. The methyl radicals combine to form ethane and are transported away from the growth region. Thus, carbon is not being incorporated into the ZnSe films from these photodissociation byproducts. The CH radicals relax to their ground state within 300 ns and likely react with H_2 to form CH_3. Due to the expected low efficiency of the photoexcitation process to make CH* and its high reactivity with hydrogen, it is likely that these radicals also do not effect the films. Thus, the use of a high energy density system in the dissociation of DMZn is beneficial to the growth process, and there are no indications that such a system produces any reasonable channels for carbon contamination.

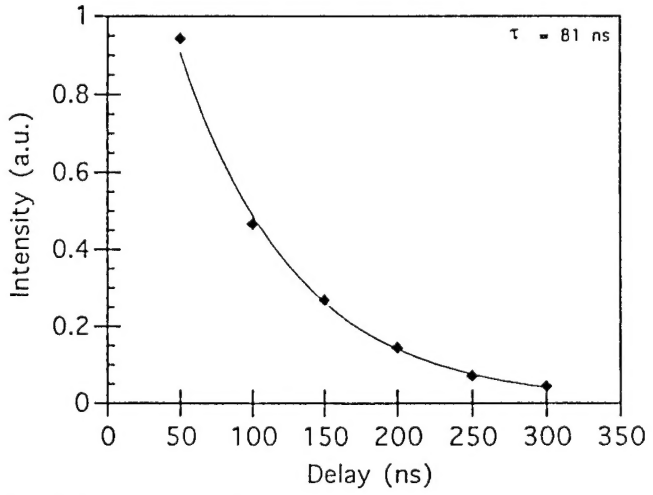

Fig. 13. Decay of the Q-Branch emission from CH*. The decay curve fits an exponential decay which gives τ = 80 ns.

ACKNOWLEDGMENT

The authors would like to thank Dr. Robert Curl and Dr. Roland Sauerbrey for valuable consultations during the work. Assistance was also provided by Dr. Frank Tittel and Dr. Paul Gillespie. Financial support was provided by Dr. Skip Porter of the Houston Advanced Research Center (HARC) and the Advantest Corporation. This work was performed under DARPA Grant #N00014-89-J-3122.

REFERENCES

1. J.M. DePuydt, M.A. Haase, J. Qiu and H. Cheng, *J. Cryst. Growth* 117, 1078 (1992).
2. T.V. Butkhuzi, A.N. Georgobiani, B.T. Eltazarov, T.G. Khulordava and M.B. Kotljarevsky, *J. Cryst. Growth* 117, 1055 (1992).
3. J.Y. Bigot, A. Daunois, R. Leonelli, M. Sence, J.G.H. Mathew, S.D. Smith and A.C. Walker, *Appl. Phys. Lett.* 49, 844 (1986).
4. G.D. Studtmann, R.L. Gunshor, L.A. Kolodziejski, M.R. Melloch, J.A. Cooper, R.F. Pierret, D.P. Munich, C. Choi and N. Otsuka, *Appl. Phys. Lett.* 54, 1249 (1988).
5. L. Wei, Y.K. Cho and C. Dosho, *Jpn. J. Appl. Phys.* I 30, 2442 (1991).
6. B. Cockayne, P.J. Wright, M.S. Skolnick, A.D. Pitt, J.O. Williams and T.L. Ng, *J. Cryst. Growth* 72, 17 (1985).
7. G.B. Shinn, P.M. Gillespie, W.L. Wilson and W.M. Duncan, *Appl. Phys. Lett.* 54, 2440 (1989).
8. R.L. Jackson, *J. Chem. Phys.* 96, 5938 (1992).
9. H. Okabe, *Photochemistry of Small Molecules.* (New York: Wiley and Sons, 1978), p. 269.

Table II. Energies of Reactions

	Dissociation Reaction			Energy	Reference
I	$Zn(CH_3)_2$	→	$Zn(CH_3) + CH_3$	2.76 eV	Jackson[35]
II	$Zn(CH_3)$	→	$Zn + CH_3$	1.06 eV	Jackson[35]
III	CH_3	→	$H + CH_2$	4.9 eV	Herzberg[16]
IV	CH_2	→	$H + CH$	4.3 eV	Herzberg[16]
V	$CH(A\,^2\Delta)$	→	$CH(X\,^2\Pi)$	2.87 eV	Barnes[31], this work
			Total Required Energy	15.89 eV	
			hυ (193 nm)	6.42 eV	

10. B. Liu, R.F. Hicks and J.J. Zinck, *J. Cryst. Growth* 123, 500 (1992).
11. K.P. Giapis, K.F. Jensen, J.E. Potts and S.J. Pachuta, *Appl. Phys. Lett.* 55, 463–466 (1989).
12. M.A. Rueter and J.M. Vohs, *Surf. Sci.* 268, 217 (1992).
13. K.P. Giapis, K.F. Jensen, J.E. Potts and S.J. Pachuta, *J. Electron. Mater.* 19, 453 (1990).
14. H. Habeeb, D.J. LeRoy and E.W. Steacie, *J. Chem. Phys.* 10, 261 (1942).
15. C.J. Chen and R.M. Osgood, *J. Chem. Phys.* 81, 327 (1984).
16. G. Herzberg, *Molecular Spectra and Molecular Structure III. Electronic Spectra of Polyatomic Molecules* (New York: Van Nostrand Co., 1966), p. 514, 609.
17. R.D. Anderson and H.A. Taylor, *J. Phys. Chem.* 56, 498 (1952).
18. A.M. Bass and A.H. Laufer, *Int. J. Chem. Kin.* 5, 1053 (1973).
19. J.I. Steinfeld, *Chemical Kinetics and Dynamics* (Englewood Cliffs, N.J.: Prentice Hall, 1989), p. 8.
20. W. Tsang and R.F. Hampson, *J. Phys. Chem. Ref. Data* 15, 1087 (1986).
21. A. Callear and H.E. van den Berg, *Chem. Phys. Lett.* 5, 23 (1970).
22. Y. Fujita, S. Fujii and T. Iuchi, *J. Vac. Sci. Tech. A* 7, 276 (1989).
23. J. Berkowitz, *Photoabsorption, Photoionization, and Photoelectron Spectroscopy* (New York: Academic Press, 1979), p. 139.
24. A. Corney, *Atomic and Laser Spectroscopy* (Oxford: Clarendon Press, 1988), p. 300.
25. A.P. Thorne, *Spectrophysics* (New York: John Wiley and Sons, 1974), p. 308.
26. C.H. Corliss and W.R. Bozman, *Experimental Transition Probabilities for Spectral Lines of Seventy Elements* (National Bureau of Standards, 1962), Monograph 53, p. 540.
27. P.J. Young, R.K. Gosavi, J. Connor, O.P. Strausz and H.E. Gunning, *J. Chem. Phys.* 58, 5280 (1973).
28. W. Kedzierski, J. Supronowicz, J.B. Atkinson and L. Krause, *Can. J. Phys.* 68, 526 (1990).
29. W.H. Breckenridge and J.H. Wang, *Chem. Phys. Lett.* 123, 17 (1986).
30. S.J. Jeans, *An Introduction to the Kinetic Theory of Gases* (New York: Cambridge University Press, 1962), p. 153.
31. R.H. Barnes, C.E. Moeller, J.F. Kircher and C.M. Verber, *Appl. Optics* 12, 2531 (1973).
32. A.P. Baronavski and J.R. McDonald, *Chem. Phys. Lett.* 56, 369 (1978).
33. W. Braun, J.R. McNesby and A.M. Bass, *J. Chem. Phys.* 46, 2071 (1967).
34. V.M. Donnelly, M. Geva, J. Long and R.F. Karlicek, *Appl. Phys. Lett.* 44, 951 (1984).
35. R.L. Jackson, *Chem. Phys. Lett.* 163, 315 (1989).